Thesis for the degree of Doctor of Philosophy

Low temperature deicing of road infrastructure using renewable energy

Josef Johnsson

Department of Architecture and Civil Engineering
CHALMERS UNIVERSITY OF TECHNOLOGY
Göteborg, Sweden 2019

Low temperature deicing of road infrastructure using renewable energy
Josef Johnsson
ISBN 978-91-7905-168-6

Doktorsavhandlingar vid Chalmers tekniska högskola
Ny serie nr 4635
ISSN 0346-718X

Department of Architecture and Civil Engineering
Chalmers University of Technology
SE–412 96 Göteborg, Sweden
Telephone + 46 (0) 31 – 772 1000

Cover: Karin Holmgren, see Figure 1.1 on page 6.

Typeset by the author using LaTeX.

Printed by Chalmers Reproservice
Göteborg, Sweden 2019

to my family and friends

Why do we fall, sir? So that we can learn to pick ourselves up.
The Dark Knight

Abstract

Winter road maintenance is costly, but it is an inevitable expense, because it is necessary to keep roads accessible and safe. Existing winter road maintenance methods in Nordic countries use 600,000 tons of salt annually. The salt ends up in the environment along the roads and results in environmental issues. This thesis proposes an alternative winter road maintenance concept for critical parts of the road infrastructure. The proposed concept consists of a hydronic heated pavement (HHP), utilised as a pavement solar collector (PSC), which is connected to a borehole thermal energy storage (BTES). The combination of an HHP and a BTES allows solar radiation to be harvested during the summer and the stored energy to be used for winter road maintenance. This system can be installed at critical parts of a road infrastructure. In existing HHPs, district heating or other high-temperature energy sources are currently used; however, high-temperature energy sources limit the implementation of HHP systems. Research on using low-temperature energy sources could result in a reduction in the primary energy requirements and make the implementation of HHP systems more feasible. This thesis aims to investigate the feasibility of implementing HHPs using renewable energy, in Scandinavian countries.

This manuscript presents experimental and numerical results from a field station consisting of a BTES-connected HHP system. The field station was constructed in 2017 and harvesting experiments were conducted during the summer of 2018. The anti-icing and de-icing functions of the HHP system were studied during the winter of 2018/2019.

The results revealed that the solar efficiency of the HHP system reach as high as 42%, and 245 kWh/m^2 of solar heat was harvested during the summer of 2018. This is a comparably high value for a PSC. The harvested energy was higher than the supplied heat (132 kWh/m^2) during the following winter. However, the cold climate at the field station required supplementary heating, as the BTES did not have the capacity to supply the required temperature of 7 $°C$ to the HHP. The numerical simulations revealed that by using dew-point regulation and weather forecasting, the energy consumption could be reduced by 62% compared to a simple air temperature regulation. Based on the experimental and numerical results, it can be concluded that it is feasible to design HHP systems to use low-temperature ($<$10 $°C$) sources and at the same time achieve a substantial improvement in the surface conditions in a Scandinavian climate.

Keywords: Hydronic heated pavements, borehole thermal energy storage, BTES, pavement solar collector, renewable energy, numerical simulations

Acknowledgments

Thanks for all the support I have received during this five-year-long journey. There are many people whom I need to send my gratitude to and this list would be too long if I were to list you all.

This journey started in 2014 when I visited Chalmers as an HVAC engineer. I had previously worked with hydronic heated pavements and then I met Bijan who was about to start this project on ice-free roads. We had a long discussion and I decided to apply for the position as a PhD candidate in his project. I am very glad that he accepted my application and since then, he has been guiding me in the world of research. If I had not applied, I would have missed out on meeting all of my fantastic colleagues. Thank you, Raheb, Christian, and Tommie for being good roomies in the old office and all my new roomies like Kaj and Pepe. Thank you, Pepe, for the discussions, hikes, and all the time spent. To the senior staff, I would like to say thank you for all that you have taught me, and I would especially like to mention Paula for the time we have worked together and Carl-Eric for being an examiner who can grasp a problem as quick as a flash. I would also like to thank Jan, Björn and Jan-Erik. Without you there would not have been a field station. Björn, we miss you.

Finally, I would like to thank my family for all their support. Emma, thank you for the understanding. Melker, I'm so glad that you are here, you arrived just 14 days before deadline of this manuscript.
Love you all!

Josef Johnsson
Göteborg, October 2019

List of Publications

This thesis is based on the following appended papers:

Paper 1. Bijan Adl-Zarrabi, Babak Ebrahimi, Mohammed Hoseini, Josef Johnsson, Raheb Mirzanamadi, Maria Taljegard. *Safe and Sustainable Coastal Highway Route E39.* Transportation Research Procedia vol. 14. 2016.

Paper 2. Josef Johnsson, Bijan Adl-Zarrabi. *Modeling the thermal performance of low temperature hydronic heated pavements.* Cold Regions Science and Technology, vol.161, 81-90, 2019.

Paper 3. Josef Johnsson, Bijan Adl-Zarrabi. *Modelling and evaluation of groundwater filled boreholes subjected to natural convection.* Applied Energy, vol.253, 113555, 2019.

Paper 4. Josef Johnsson, Bijan Adl-Zarrabi. *Pavement solar collector for the northern hemisphere.* Under review Applied Energy (2019), vol.xxx, xx-xx. 2019.

Other relevant publications authored or co-authored by Josef Johnsson:

Josef Johnsson, Bijan Adl-Zarrabi. *Hydronic Pavement for Ice-Free Bridges.* In XVth International Winter Road Congress, Gdansk: 2018.

Raheb Mirzanamadi, Carl-Eric Hagentoft, Pär Johansson, and **Josef Johnsson**. *Anti-Icing of Road Surfaces Using Hydronic Heating Pavement with Low Temperature.* Cold Regions Science and Technology 145: 106–18. 2018.

Josef Johnsson. *Winter Road Maintenance Using Renewable Thermal Energy.* Lic Thesis 2017:3. Göteborg: Chalmers University of Technology, 2017.

Josef Johnsson. *Winter road maintenance a review: Literature Review.* Report 2017:4, Göteborg: Chalmers University of Technology, 2017.

Esben Almqvist, **Josef Johnsson**. *Identifying critical road sections related to winter road maintenance.* Report 2017:5, Göteborg: Chalmers University of Technology, 2017.

Josef Johnsson, Bijan Adl-Zarrabi. *Hydronic pavement using low temperature borehole thermal energy storage*. Presented at Advances in Civil, Environmental and Materials Research (ACEM16). South Korea, 2017.

Bijan Adl-Zarrabi, Raheb Mirzanamadi, **Josef Johnsson**. *Hydronic Pavement Heating for Sustainable Ice-free Roads*. Transp. Res. Procedia 14, 704–713. doi:10.1016/j.trpro.2016.05.336, 2016.

List of Acronyms

STES	–	Seasonal Thermal Energy Storage
BTES	–	Borehole Thermal Energy Storage
PSC	–	Pavement Solar Collector
HHP	–	Hydronic Heated Pavement
ME	–	Mean Error
RMSE	–	Root Mean Squared Error
CFD	–	Computational Fluid Dynamics
FEM	–	Finite Element Method
FDM	–	Finite Difference Method
HyRoSim	–	Hydronic Road Simulation
TPS	–	Transient Plane Source
WRM	–	Winter Road Maintenance

Contents

Part I

Introductory chapters

Chapter 1

Introduction

Traffic safety is a global challenge, with more than 1.2 million fatalities worldwide, making road traffic accidents the main cause of death for young people. Annually, 50 million people suffer from non-fatal traffic accidents. The global financial cost for these traffic accidents is estimated to reduce the GDP by 3% (WHO 2015). During recent years, the number of fatalities has been constant, while global traffic has been increasing. This indicates that global traffic safety measures are effective for reducing the rate of fatalities.

Globally, traffic safety during winter conditions is not a major problem. However, in countries with harsh winters such as the Scandinavian countries, winter conditions are considered as a major safety issue. It is well known that driving during winter conditions is more dangerous, owing to the increased risk of accidents, compared to driving under bare-road conditions (A. K. Andersson 2010; Johansson 2000; Norrman et al. 2000; Wallman et al. 1997). The increased probability of accidents during winter conditions motivates traffic safety measures to mitigate slippery conditions on the road surface. These measures may be even more important in the future, as climate change could lead to a small increase in the number of accidents (A. K. Andersson 2010).

Winter road maintenance (WRM) has been found to be effective to counter the increased accident risk during winter conditions (Kuemmel and Hanbali 1992; Norrman et al. 2000; Usman et al. 2010). Modern WRM consists of different winter maintenance activities, aiming at either snow and ice removal, or friction control. Snow removal aims at maintaining the accessibility of roads and keeping them open to traffic, whereas friction control aims at fostering safety by maintaining the friction between the tires of the vehicle and the road surface. The most common winter maintenance activity in the Scandinavian countries is friction control, which is typically done by spreading either one or both, of the following: (i) a freezing point depressant such as sodium chloride (salt) or (ii) an abrasive such as sand (Klein-Paste 2008; Lysbakken 2013; Minsk 1998). WRM and the usage of salt and abrasives has been proved to be effective in reducing the risk of accidents. Nonetheless, the use of salt has been questioned. Further details and issues related to WRM can be found in (Johnsson 2017a).

Annually, the Nordic countries spread 600,000 tons of salt and 1,800,000 tons of

abrasives on the roads, at a financial cost of approximately 6,400 million NOK/year (2015) (Arvidsson et al. 2018). This salt commonly ends up in the environment along the road, causing damage to vegetation, saltification of fresh water, and facilitating leaching of toxic heavy metals (Fay and Shi 2012). The abrasives used are mainly sand or crushed rocks, which are finite resources. Furthermore, the use of abrasives is connected to environmental issues such as an increase of fine PM10 particles in the air (Ketzel et al. 2007). The fine particles originating from abrasives and traffic-related emissions halve also been connected to health risks in numerous studies (Valavanidis et al. 2008). To summarise, WRM is costly (Knudsen et al. 2016), but the societal benefits from WRM are much greater than the costs (Kuemmel and Hanbali 1992). However, there are local environmental concerns that must be addressed.

A common environmental concern related to WRM is the saltification of freshwater streams, which are typically located at low points in the landscape. Roads passing through these low points are predisposed to suffer from slippery road conditions (Lindqvist et al. 1983), as these sites would have higher dew point temperatures and lower air temperatures. Other parts of the road infrastructure with increased risk for slippery road conditions include bridges and highway junctions, because these structures lack the thermal heat flow from the underground. If these sites could be ice-controlled by alternative means, the CO2 emissions from winter maintenance could be reduced (Nordin 2015; Ye et al. 2013).

A more environmentally friendly approach is to use thermal methods for local WRM. Thermal methods imply the addition of thermal energy to the pavement by means of a surface heating system, thereby melting ice and snow on the road. Such methods are suitable for both friction control and snow and ice removal, as they create a bare road surface (Lysbakken 2013). Research on hydronic heated pavements (HHPs) has been performed since the introduction of the technology in 1948 in Oregon, USA (Adlam 1950; John W Lund 2000; Magnusson 1977; Pan et al. 2015). An HHP consists of a pipe network embedded in the pavement. A warm fluid is circulated in the pipes, thereby facilitating the transport of thermal energy into the pavement. Frequently used energy systems include gas boilers and district heating, which restricts the suitable sites for HHP systems and the environmental gains. Reductions in the environmental impact of HHP systems could be achieved if HHP systems were to use renewable energy sources.

Solar thermal energy is a renewable energy source that is available in abundance. In 1994, an HHP system that utilised solar energy was installed on a bridge near Därlingen in Switzerland (Eugster 2002; Eugster 2007; John W Lund 2000). This project, SERSO, proved the feasibility of such a system (Pahud 2007). They overcame the obvious problem associated with using solar energy in the winter by merging a seasonal thermal energy storage with an HHP system. The working principle of the system used in the SERSO project can be divided into three parts: (I) During summer, the solar radiation heats the pavement and by the embedded pipe network, the heat is harvested and transferred to a seasonal thermal energy storage. (II) The system is dormant when no more heat could be gained from the pavements surface. (III) When there is a need for anti-icing and friction control, the pumps are started and the stored heat is transferred to the pavement, thereby mitigating the slippery

conditions.

This thesis will investigate the feasibility of an HHP system using renewable energy in a Scandinavian climate.

1.1 Project background

In 2013, a collaboration was established between Chalmers University of Technology and the Norwegian Public Road Administration (NRPA), aiming at supporting the Norwegian road project E39 Coastal Highway Route. The road project aims at improving the existing E39 and replacing ferry connections with fixed connections, thereby reducing the travel time from 21 to 11 hours. One of the focus areas of the collaboration is to investigate how the Coastal Highway Route E39 could become carbon neutral and how infrastructure can be utilised for energy production (Adl-Zarrabi et al. 2016; Chalmers University of Technology 2013; Statens Vegvesen 2013). The NRPA initiated the research area 'Safe and ice-free bridges using renewable thermal energy sources', with the main concept of utilising renewable thermal energy to mitigate slippery conditions on roads.

At the same time, the Swedish Transport Administration (Trafikverket), was fostering the idea of developing their winter road maintenance methods by using heated pavement surfaces. Trafikverket had funded a pilot study on how solar energy could be utilised for the de-icing of critical parts of the road infrastructure (Orring 2012; Sundberg 2012). The pilot study identified a number of successful international examples and suggested further studies in a Nordic climate. In 2014, the results of those studies were published and revealed that a system utilising the pavement as a pavement solar collector (PSC) in combination with a borehole thermal energy storage (BTES) system would be a feasible solution (Sundberg and Lidén 2014). However, Sundberg concluded that further research and testing would be needed to validate the concept.

The concept for a renewable HHP system, proposed by this thesis, is based on the SERSO project, and is presented in Figure 1.1. The road section with the HHP has an embedded pipe network, similar to a modern underfloor heating system. A heat transfer fluid is circulated through the pipes, transferring heat to the pavement surface from an energy source. The energy source can vary, depending on the available sources at the site. Possible sources include low-temperature (10 $^{\circ}C$) industrial waste heat, ground water, sea water, or a seasonal thermal energy storage. The system is activated based on control settings and weather parameters measured by the local weather station.

The proposed HHP system connected to a BTES faces a number of challenges that must be addressed. By using solar energy, the system is dependent on a BTES owing to seasonal variations in the amount of incoming solar radiation. In order for a BTES to be effective, the losses from the storage need to be low. This can be achieved by reducing the temperature levels used in HHP system, because the temperature differences drive heat losses. However, low temperatures reduce the amount of heating power that can be extracted from a BTES, and the pavement requires a certain amount of heating power to maintain the surface temperature. The

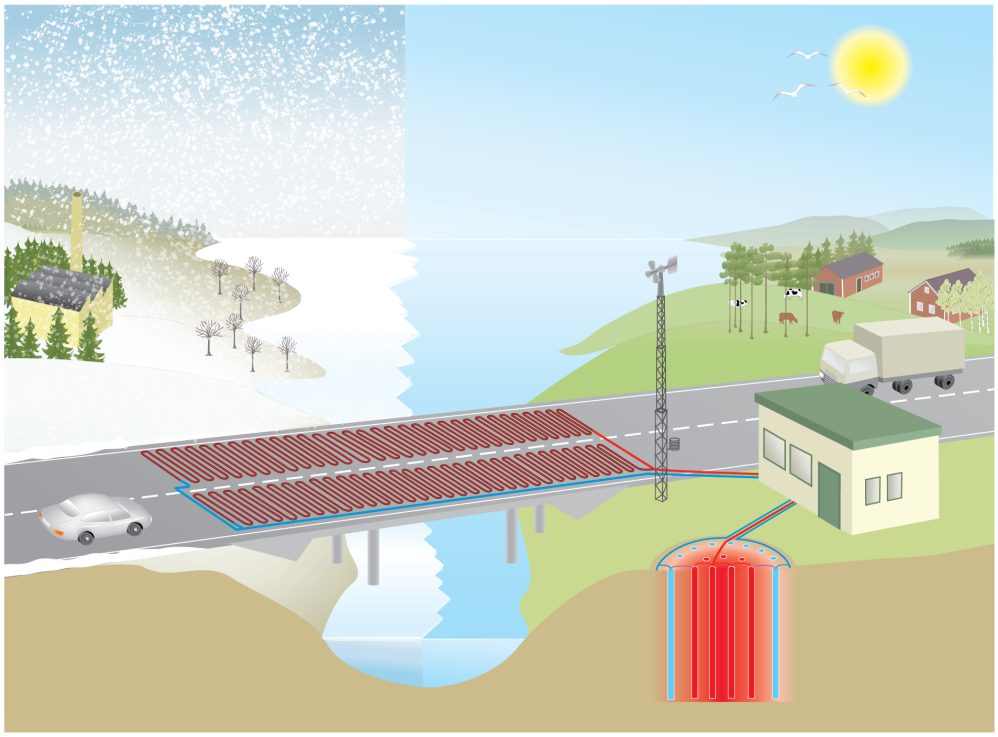

Figure 1.1: Concept of the studied system, the hydronic pavement is connected to a thermal energy storage keeping the harvested solar energy from the summer into the winter. (Karin Holmgren)

low temperatures can partly be compensated for by modifying the pipe positions and thermal conductivity of the pavement, or by adjusting the control system. The control system needs to take the low supply temperature into account, which can be achieved by starting the system in a timely manner based on weather forecasts. By extending the period during which the system is operated, a lower mean heating power can be used. In order to achieve a functioning system, this whole chain of challenges must be addressed.

1.2 Scope of work

This thesis focusses on the feasibility of using solar powered HHPs in a Scandinavian climate, as a part of the 'safe and ice-free bridges using renewable thermal energy sources' research area.

The aim of this thesis is to investigate the function of an HHP system by both numerical and experimental methods. The goal of this system is to use a pavement as a solar collector, store the harvested energy in a BTES, and finally use the stored energy to de-ice the road surface. The objective of this work is to develop a concept for the system and validate it by theoretical and experimental studies. The experimental studies are performed both in the laboratory and in an operational environment, i.e. at a field station.

1.3 Limitation

This thesis is based on experimental results from one field station in Sweden. The field station was constructed as a real road. However, the traffic and winter maintenance on the road do not represent real conditions. This reduces the effect that traffic has on the surface conditions and it also means that the winter maintenance is not as frequent as on a normal road.

This study focusses on the thermal performance of the system and does not investigate the mechanical durability of the HHP system.

1.4 Methodology

This thesis is based on experimental and numerical methods. A field station for an HHP system was constructed and operated for one year. The lessons learned from the first year will be used in the following years, and the data collected were used to verify a numerical model developed in this work. This numerical model, 'HyRoSim', has been used to investigate the influence of different parameters on the performance of the HHP system.

1.5 Application of HHP systems

HHPs have been used since 1948 (Adlam 1950), and it is estimated that 2,500,000 m^2 are heated by HHP systems worldwide (John W. Lund and Boyd 2016). Today, the main users of HHP systems in Sweden are municipalities, which mainly use them for snow melting in city central areas. It has been found that HHP systems have a preventing effect on the number of injuries due to slipping (Carlsson et al. 2018). Furthermore, the usage of HHP systems in city central areas reduces the need for abrasives such as sand. The reduced usage of sand further reduces the risk of falling and less sand also reduces the need for maintenance of floors and escalators (Carlsson et al. 2018).

Today, it is estimated that more than 400,000 m^2 of HHP systems are operational in Sweden, but there is still a lack of systematic knowledge on the operational usage, energy consumption, and the operating costs of the systems. This lack of knowledge is evident from the study by Carlsson et al. They contacted 20 larger cities in Sweden and asked for information on HHP systems. Based on their responses, only half of the cities could provide basic information (see Table 1.1). This suggests that the municipalities give their surface heating systems a low priority, which could indicate a potential for energy savings.

Winter maintenance is not only related to roads, as snow and ice need to be removed from other areas and infrastructure as well. Traditional WRM (Johnsson 2017a) i.e. by using mechanical snow removal and salt, is the recommended method for maintaining the majority of the infrastructure. However, for certain locations, alternatives such as HHP systems should be considered (Nordin 2015). In Table 1.2, different locations for HHP systems are presented. Other locations might also

Table 1.1: Basic information of cities in Sweden with hydronic heating systems (Carlsson et al. 2018).

City	Heated Area m^2	From	City	Heated Area m^2	From
Stockholm	100,000	1970s	Gävle	-	-
Göteborg	-	1979	Eskilstuna	-	1960s
Uppsala	-	-	Karlstad	-	1979
Örebro	-	-	Borås	28,000	-
Helsingborg	-	2007	Södertälje	-	1970s
Jönköping	4,800	2000s	Linköping	33,000	1970s
Umeå	21,600	1974	Västerås	150,000	1960s
Norrköping	-	-			

be suitable. However, for road infrastructure, it is recommended to focus on steep slopes and bridges, which have both been identified as critical locations (Almkvist and Johnsson 2017). In the study by Almkvist and Johnsson, locations along a road were identified and classified based on the likelihood for slipperiness. Based on weather data, a few hot-spots could be identified. However, these locations could have been identified instead by qualitative measures, as it is known that bridges can suffer more from slipperiness and also that locations near road weather stations are known to experience more hours of slipperiness. Nonetheless, for new roads, it is useful to use numerical software, such as the one in the paper by Almkvist and Johnsson to identify critical locations for slipperiness.

One way of identifying possible locations for HHP systems is to perform a qualitative interview-based study with the local road authorities and winter road contractors. They have detailed information on the status of the road surface and can identify locations that would benefit from an HHP system. Based on these locations, a detailed cost–benefit analysis can be performed based on, e.g. local conditions and distance to maintenance depot.

Table 1.2: Suitable locations for HHP systems, modified from (Sundberg and Lidén 2014).

Application	Locations	Comment
Roads	Steep slopes	Enhance traffic flow by preventing heavy vehicles from getting stuck.
	Bridges	Reduce accident risk due to sudden changes in surface conditions due to frost and black ice.
	Highway junctions	Snow removal in order to reduce the need for unnecessary driving with snow ploughs.
	Tunnel entrances	Snow removal in front of long tunnels in order to remove unnecessary driving with snow ploughs.
	Fresh water sources	Reduce the salt usage near sensitive fresh water sources.
Railways	Railway switch	Snow removal to keep the railway switches operating during snow fall.
	Railway platform	Snow and ice removal from railway platforms due to lack of accessibility by snow removal vehicles.
Airports	Parking areas	Snow removal from parking areas for aircraft in order to reduce the risk of plane–vehicle collisions.
Pedestrians	Shopping/main streets	Snow removal and reduced risk of falling, increased accessibility.
	Bus stops	Snow removal during winter but also reduction in pavement temperatures during summer, which reduces the risk of rutting.

Chapter 2

Theoretical studies

This chapter covers the initial studies on the harvesting potential of hydronic pavements and the development and usage of a numerical model for HHP systems, called 'HyRoSim'.

2.1 Initial harvesting potential

The amount of energy that can be harvested is of interest, because that sets an upper limit on how much energy an HHP system can deliver. If the energy is insufficient, supplementary energy sources will be needed.

A preliminary study on the amount of energy that can be harvested was presented in Paper 1 and more details were presented in (Johnsson 2017b). The preliminary literature review found that approximately 30% of the incoming solar radiation can be harvested ($\eta_{PSC} = 0.3$). Based on the assumption of $\eta_{PSC} = 0.3$, the harvesting potential for different locations in Scandinavia and the city of Luzern (location for the SERSO project) were calculated (see Figure 2.1). It is evident that there is a small variation in the harvesting potential, with a mean potential of 131 kWh/m^2 and a standard deviation of 7.5 kWh/m^2. Based on this preliminary study, it can be concluded that solar radiation is available as an energy source in large parts of Scandinavia, with only small variations.

2.2 Model development

Based on the initial studies on the energy harvesting potential and on the usage of BRIDGESIM, it was concluded in (Johnsson 2017b) that a model for HHP systems should take the dew point into account, as well as a BTES. None of the models investigated in (Johnsson 2017b) considered surface moisture and BTES systems. Owing to the lack of available models, HyRoSim was developed as a model for HHP systems.

HyRoSim consists of two modules, as illustrated in Figure 2.2: the HHP module (left) and the storage module *Pygfunction* (right) developed by Cimmino and modified by the author in Paper 3. The software *Pygfunction* is an open-source software

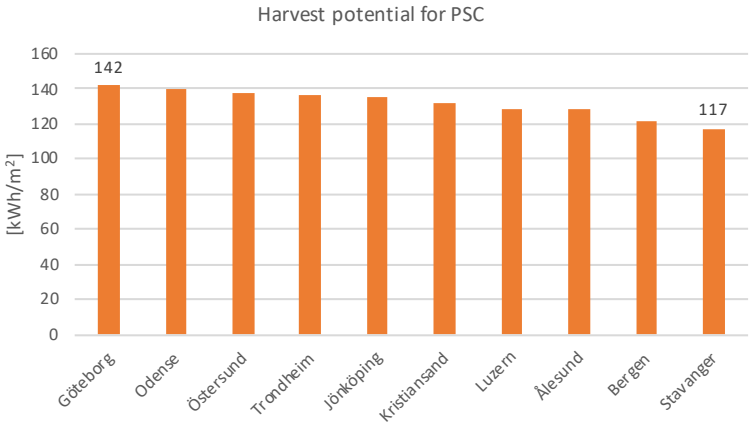

Figure 2.1: Potential for energy harvesting by a PSC during the summer based on the assumption of $\eta_{PSC} = 0.3$.

package based on the work by (Cimmino and Bernier 2014) and (Cimmino 2017). The software calculates fluid and borehole wall temperatures for a borehole field, based on the heat load applied to the storage. By combining *Pygfunction* with the HHP module presented in Paper 2, a model for an HHP system was created that can handle surface moisture and BTES.

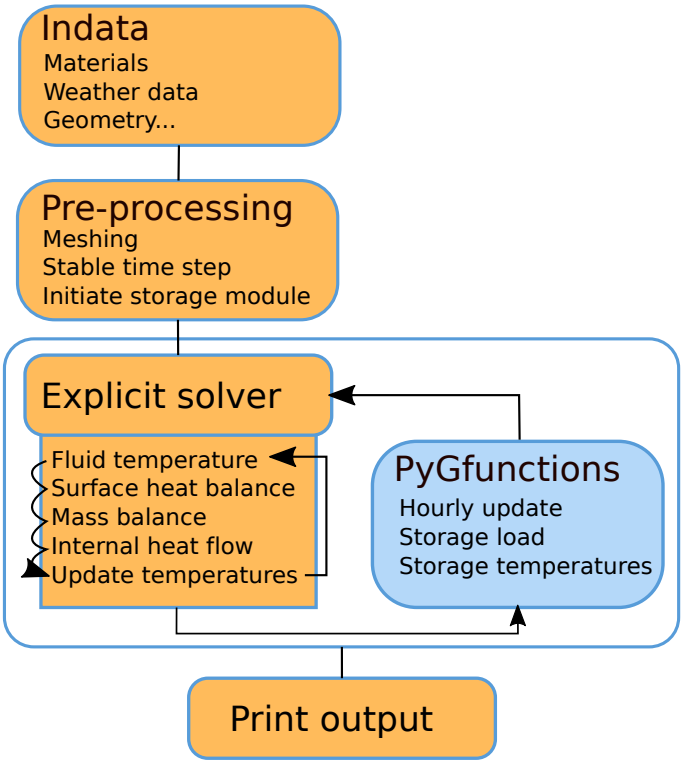

Figure 2.2: Flow chart for the simulation tool HyRoSim used in this study.

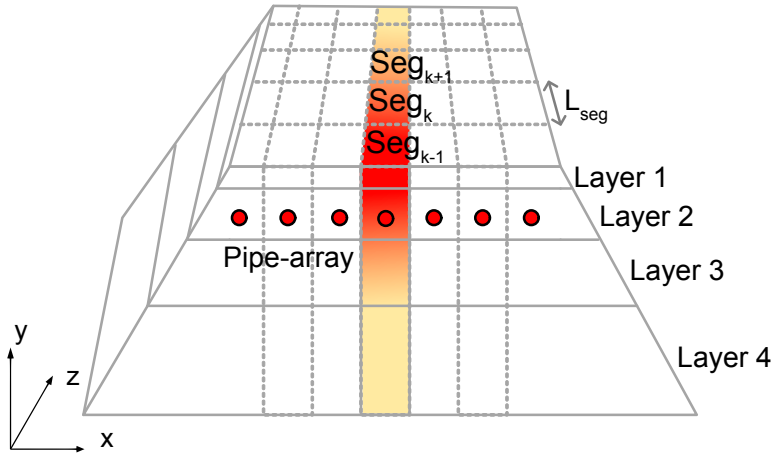

Figure 2.3: Hydronic heated pavement divided into segments along the longitudinal fluid flow axis (z). The HHP model represents the centrally shaded volume.

2.2.1 Hydronic heated pavement module - Introduction

The HHP module was developed to calculate the heat flows and surface conditions representing a real HHP system. A sketch of the studied problem and its geometrical model consisting of a road with an embedded parallel-pipe array is presented in Figure 2.3. The upper pavement layer is exposed to the outdoor climate, and the lower boundary could either be adiabatic or have a fixed temperature. The geometrical model consists of several horizontal layers with different thermal properties. In the longitudinal z-direction, the geometrical model is divided into a number of segments (Seg), each having the same thermal properties. The model represents a centrally placed pipe in an infinite pipe array. In each segment, the heat transfer from the fluid to the surrounding pavement is calculated by using the finite difference method (FDM). The thermal connections between the subsequent segments (z-direction) are represented by the convective heat transfer in the pipes (see Section 2.2.4). The HHP module was developed in the platform-independent programming language Python 3.5.2.

The HHP module calculates the fluid temperatures and the surface conditions for a centrally placed pipe, as seen in Figure 2.3. The full 3D domain of the problem calculated by the HHP module is represented by Figure 2.4. The 3D domain is divided into segments (Seg_k) along the z-direction. The size of the segments depends on the pipe spacing, cc [m], and the length of each segment, L_{seg} [m].

For each segment (Seg_k), the heat transfer in the domain is solved using the FDM. The domain is represented by a section in the xy-plane, which is separated into two regions (see Figure 2.5, left). Near the pavement surface, there is a 2D domain containing the upper pavement layers and the pipe inclusion cells. The heat transfer in this region is 2D, owing to the heat flux from the embedded pipe over the boundary F-E. Deeper in the domain, the heat flux is 1D, owing to the lower thermal influence from the pipe. Therefore, the deeper layers of the pavement structure are represented by a 1D-domain. This reduces the number of calculation cells in the

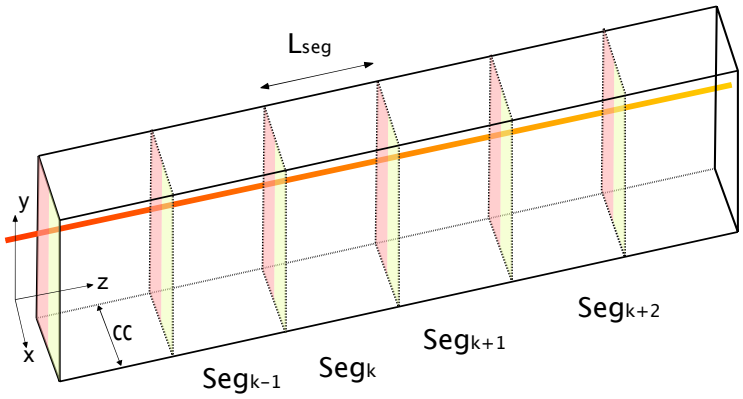

Figure 2.4: Geometrical model of 3D domain with segments used for the fluid temperature calculations.

domain, thereby reducing the calculation time. To further reduce the calculation time, symmetry is assumed along the central axis, (A-D) in Figure 2.5 (left). This reflects the assumption of no heat flux between the right- and left-hand sides.

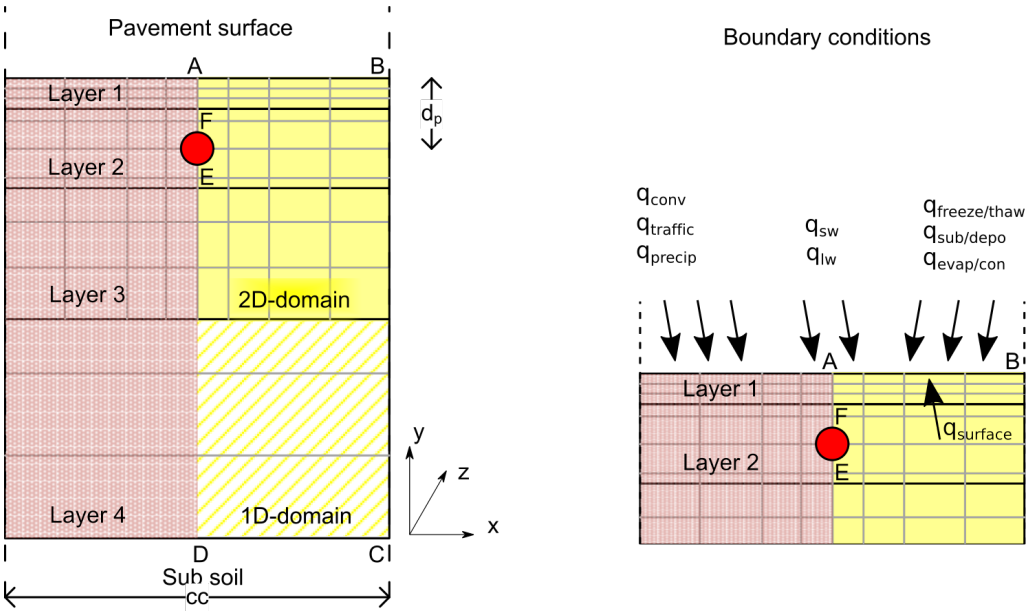

Figure 2.5: Left: Section plane representing segment, Seg_k, and the domain studied using FDM. The domain is divided into 1D and 2D regions. Right: Boundary conditions affecting the pavement surface.

2.2.2 Internal heat balance

The HHP module uses the FDM to calculate the energy flows within the pavement. The internal heat balance in each segment is solved using the energy balance method, which assumes that all energy fluxes in and out of a cell must be equal to the

change of energy in the cell. Mathematically, this is described as the general partial differential equation for heat transfer and conservation of energy.

$$\rho\, C_p \frac{\partial T}{\partial t} = \lambda \cdot \left(\frac{\partial^2 T}{\partial x^2} + \frac{\partial^2 T}{\partial y^2} \right) + q \tag{2.1}$$

Equation 2.1 is solved using the scheme described by Karlsson (2010). The solution is based on a finite difference discretisation, stating that for every time step (n) with a time length (Δt), the energy balance should be maintained (Hagentoft 2001). The heat balance equation 2.1 is discretised as:

$$\begin{aligned} C_{i,j} \frac{T_{i,j}^{n+1} - T_{i,j}^{n}}{\Delta \mathrm{t}} = \Big[& K_{i,j}^{x}(T_{i-1,j} - T_{i,j}) + K_{i+1,j}^{x}(T_{i+1,j} - T_{i,j}) + K_{i,j}^{y}(T_{i,j-1} - T_{i,j}) \\ & + K_{i,j+1}^{y}\left(T_{i,j+1} - T_{i,j}\right) + q_{i,j}^{source} \Big]^{n} \end{aligned} \tag{2.2}$$

where the domain is divided into calculation cells. The cells are indexed by i in the horizontal direction and j in the vertical direction, as illustrated in Figure 2.6. Each cell has an individual heat capacity (C) and temperature (T). The source term (q) is used for the cells that contain the pipe and those on the boundary A-B. Cells are thermally connected to their adjacent cells by the thermal conductance (K). The thermal conductances between cells are calculated as:

$$\begin{aligned} K_{i,j}^{x} &= \frac{d_{i,j}^{y}}{\frac{d_{i-1,j}^{x}}{2\lambda_{i-1,j}} + \frac{d_{i,j}^{x}}{2\lambda_{i,j}}} [\frac{\mathrm{W}}{\mathrm{m\ K}}] \\ K_{i,j}^{y} &= \frac{d_{i,j}^{x}}{\frac{d_{i,j-1}^{y}}{2\lambda_{i,j-1}} + \frac{d_{i,j}^{y}}{2\lambda_{i,j}}} [\frac{\mathrm{W}}{\mathrm{m\ K}}] \end{aligned} \tag{2.3}$$

2.2.3 Boundary conditions

The domain is exposed to external heat fluxes at three boundaries, as shown in Figure 2.5 (right). First, the heat flux over the pavement surface covering the distance from A to B. Second, the heat flux towards the subsoil C-D, and thirdly, the heat flux over the pipe boundary E-F. The other sides, B-C, D-E, and F-A have adiabatic boundary conditions.

The pavement surface is influenced by a number of heat transfer processes (see 2.5, right). These heat transfer process are: conductive heat transfer involving the heat transfer from the underground to the surface and pipes embedded in the pavement ($q_{surface}$), convective heat transfer by ambient air (q_{conv}), sensible heat from precipitation such as rain or snow (q_{precip}), sensible heat from the traffic ($q_{traffic}$), longwave radiation (q_{lw}), shortwave radiation (q_{sw}), latent heat due to evaporation and condensation ($q_{evap/con}$), latent heat due to sublimation and deposition ($q_{sub/depo}$), and latent heat due to freezing and thawing of moisture on the road surface ($q_{frezze/thaw}$) (Chen et al. 2019). The total heat balance on the road surface is calculated as

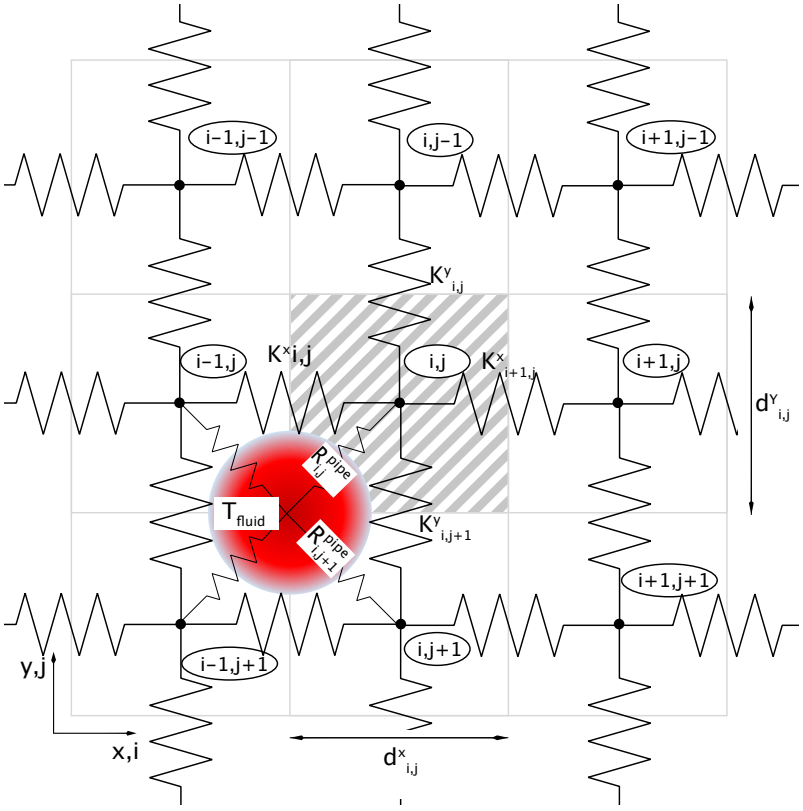

Figure 2.6: Thermal network representing the problem solved by using an explicit forward difference method.

$$0 = q_{surface} + q_{conv} + q_{precipitation} + q_{lw} + q_{sw} + q_{evap/con} + q_{sub/depo} + q_{freeze/thaw} + q_{traffic} \tag{2.4}$$

All the heat transfer parameters presented in Equation 2.4 have an influence on the pavement surface and the surface conditions. However, the surface heat balance is commonly simplified by excluding some of these parameters, such as the sensible heat from the traffic $q_{traffic}$. Therefore, $q_{traffic} = 0$ $[W/m^2]$, as it is considered negligible. Different simplifications can be made depending on which phenomena are studied, and the HHP module can handle different assumptions.

The heat flux through the top pavement layer is calculated based on Fourier's law as follows:

$$q_{surface} = \lambda \cdot \frac{\partial T}{\partial y} \tag{2.5}$$

where λ is the thermal conductivity of the pavement material, ∂y is the cell distance $[m]$, and ∂T is the temperature difference between the surface cell and the cell at a depth of ∂y $[m]$ from the pavement surface.

The convective heat flux q_{conv} $[W/m^2]$ is calculated as

$$q_{conv} = h_c \cdot (T_{ambient} - T_{surface}) \tag{2.6}$$

where $T_{ambient}$ is the ambient air temperature and $T_{surface}$ $[^{\circ}C]$ is the pavement surface temperature. The convective heat flux depends on the convective heat transfer coefficient h_c $[W/(m^2 \cdot K)]$, based on the wind speed v $[m/s]$ (Hagentoft 2001). The heat flux due to precipitation $q_{precipitation}$ $[W/m^2]$ is calculated as

$$q_{precipitation} = \dot{m}_{precipitation} \cdot C_{precipitation} \cdot (T_{ambient} - T_{surface}) \tag{2.7}$$

where $\dot{m}_{precipitation}$ $[kg/(m^2 \cdot s)]$ is the mass flow of precipitation and $C_{precipitation}$ $[J/(kg \cdot K)]$ is the heat capacity of the precipitation, which depends on whether the precipitation is in the form of snow or rain.

The net long-wave radiation, q_{lw} $[W/m^2]$, is calculated as the difference between the incoming and outgoing long-wave radiation. The procedure used is the same as that presented by Denby et al. (2013), and is calculated as

$$\begin{aligned} q_{lw} = \quad & F_{skyview} \cdot \epsilon_{sky} \cdot \sigma \cdot T_{ambient}^4 + (1 - F_{skyview}) \cdot \sigma \cdot T_{ambient}^4 \\ & - \epsilon_{surface} \cdot \sigma \cdot T_{surface}^4 \end{aligned} \tag{2.8}$$

where $F_{skyview}$ $[-]$ is the sky view factor, which is a measure of how much of the pavement is exposed to the sky. For an open field without obstructions, the value of $F_{skyview}$ would be one (1). σ is the Stefan–Boltzmann constant and ϵ $[-]$ is the emissivity of the radiating surface. The emissivity of the sky is calculated as

$$\epsilon_{sky} = \epsilon_{clear-sky}(1 - n_{cloud}^2) + \epsilon_{cloud} \cdot n_{cloud}^2 \tag{2.9}$$

where the emissivity of a cloudy sky is estimated to be approximately 0.97 $[-]$ and n_{cloud} $[-]$ is a measure of the number of clouds in the sky. The emissivity of the clear sky is calculated based on (Konzelmann et al. 1994) and presented in Paper 2.

The short-wave radiation q_{sw} is based on measured values of the incoming radiation I $[W/m^2]$, and is reduced based on the albedo α_1 $[-]$ of the pavement surface.

$$q_{sw} = (1 - \alpha_1) \cdot I \tag{2.10}$$

where α_1 varies over the day depending on the position of the sun. For further details on the varying albedo, see (Sass 1992) and Paper 2.

The latent heat is determined by the moisture mass balance on the pavement surface, and is calculated according to Denby et al. (2013). The latent heat due to freezing and thawing of water is calculated as

$$q_{freeze/thaw} = L_{fusion}\dot{m}_{melt/frezze} \tag{2.11}$$

where $L_{fusion}[J/kg]$ is the latent heat of fusion for water and $\dot{m}_{melt/freeze}$ is the freezing or melting rate of water $kg/(m^2 s)$.

The latent heat due to evaporation and condensation is calculated as

$$q_{evap/con} = L_{vaporisation}\dot{m}_{evap/con} \tag{2.12}$$

where $L_{vaporisation}[J/kg]$ is the latent heat of fusion for water and $\dot{m}_{evap/con}$ is the evaporation or condensation rate of water $kg/(m^2 s)$.

The latent heat due to sublimation is calculated as

$$q_{sub/depo} = L_{sublimation}\dot{m}_{sub/depo} \tag{2.13}$$

where $L_{sublimation}[J/kg]$ is the latent heat of sublimation for vapour and $\dot{m}_{sub/depo}$ is the sublimation or deposition rate of vapour $kg/[m^2s]$.

Mass balance

The mass balance of the pavement surface must be tracked to maintain an energy balance for the surface and to estimate the surface condition of the road. The mass balance is based on the work of Denby et al. (2013). The mass balance is separated into two parts, one for ice and one for water. The mass balance for the water on the pavement surface is calculated as

$$\frac{dm_{water}}{dt} = \dot{m}_{rain} + \dot{m}_{cond} + \dot{m}_{spray} + \dot{m}_{melt} + \dot{m}_{runoff} \tag{2.14}$$

where m_{water} is the amount of water on the pavement $[kg/m^2]$, $\dot{m}_{rain}$ is the amount of rain falling on the pavement $[kg/(m^2s)]$, $\dot{m}_{cond}$ is the amount of water added to the surface or removed by condensation $[kg/(m^2s)]$, $\dot{m}_{runoff}$ is the amount of water removed by drainage of the pavement surface $[kg/(m^2s)]$, $\dot{m}_{spray}$ is the amount of moisture removed by the vehicle spray owing to tyre–pavement interaction $[kg(m^2s)]$, $\dot{m}_{melt}$ is the amount of water added to the surface owing to the melting of ice $[kg/(m^2s)]$. The maximum amount of water on the surface is limited by the runoff from the pavement to not exceed 0.3 mm of water, which represents a road with good runoff.

The mass balance for the m_{ice} $[kg/m^2]$ is treated similarly to the water, and is calculated as

$$\frac{dm_{ice}}{dt} = \dot{m}_{snow} - \dot{m}_{sub} - \dot{m}_{melt} \tag{2.15}$$

where $\dot{m}_{snow}$ is the amount of snowfall on the pavement $[kg/(m^2s)]$, $\dot{m}_{sub}$ is the reduction in the amount of ice by sublimation $[kg/(m^2s)]$. The amount of melted ice $\dot{m}_{melt}$ is given as an addition to the water balance $[kg/(m^2s)]$ in equation 2.14. The maximum amount of snow is limited to 1 cm, representing a road that has high demands on the amount of allowed snow on the pavement surface, such as the studied road section.

Condensation and sublimation are calculated in a similar way and only differ depending on the surface temperature. For temperatures below 0 $°C$, only sublimation and deposition occur. The mass flux due to condensation and sublimation is calculated as

$$-\dot{m}_{sub} = \dot{m}_{cond} = \frac{h_c}{\rho c_{pa}}(v_{ambient} - v_{surface}) \tag{2.16}$$

where h_c $[W/(m^2 \cdot K)]$ is the convective heat transfer coefficient, $\rho_a cpa$ is the volumetric heat capacity of air $[J/(m^3K)]$, and v is the vapour content of the ambient air and at the pavement surface $[kg/m^3]$ (Hagentoft 2001).

The mass of water on the surface that is melting or freezing is based on the heat flux on the surface and the heat of fusion. It is assumed that the heat flux first affects the water/ice on the surface, which will limit the maximum surface temperature to 0 $^{\circ}C$ until all the ice is melted. The amount of melting water is calculated as

$$\dot{m}_{melt} = (q_{conv} + q_{precipitation} + q_{lw} + q_{sw})/L_{fusion} \tag{2.17}$$

where L_{fusion} $[J/(kgK)]$ is the latent heat of fusion for water. When the heat flux is positive and ice is present, there will be melting. Conversely, with a negative heat flux and water present, there will be freezing. This process is limited by the available amounts of water and ice.

The water transport due to vehicle spray $\dot{m}_{spray}$ is based on the procedure presented by Denby et al. (2013), and is calculated as

$$\dot{m}_{spray} = m_{water} R_{spray}/dt \tag{2.18}$$

where the reduction factor due to spraying R_{spray} $[-]$ depends on the number of passing vehicles, the speed of the vehicles, and number of lanes. More details are available in Paper 2

2.2.4 Pipe–pavement interaction

The HHP module uses a coupling between the fluid in the pipe and the 2D region, which is based on a procedure developed for floor heating systems by Karlsson (2010). The procedure uses a local analytical solution of the fluid temperature for each individual segment, and the fluid is step-wise exposed to the conditions in each segment. To maintain an energy balance, the resulting change in energy of the fluid in each segment is given as the heat source term to the pipe inclusion cells. A brief introduction is presented here; for more details, see Paper 2 and (Karlsson 2010).

In order to calculate the heat flux (q_f^k) into one segment indexed by k, Seg_k, as presented in Figure 2.4, the outlet fluid temperature in each segment is calculated based on a local analytical solution according to

$$T_f^k = T_0^k + \left(T_f^{k-1} - T_0^k\right) e^{-L_{seg}/l_c} \tag{2.19}$$

where T_0^k $[^{\circ}C]$ is the equivalent temperature that the pipe is exposed to in segment k, T_f is the fluid temperature in the pipe $[^{\circ}C]$, and L_{seg} is the length of the segment [m]. l_c is the characteristic length [m] of the pipe, which depends on the heat transport in the z-direction and the transverse heat losses. For details on how to calculate T_0^k and l_c, see Paper 2.

By calculating the outlet fluid temperature, T_f^k in each segment, the resulting heat flux from the pipe can be calculated. The heat flux from one segment, q_f^k $[\frac{W}{m}]$, is calculated as

$$q_f^k = \frac{\dot{m}_{flow} \cdot c_f \left(T_f^{k-1} - T_f^k\right)}{L_{seg}} \tag{2.20}$$

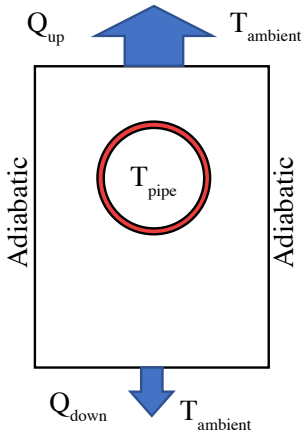

Figure 2.7: Schematic representation of validation case of a pipe embedded in a rectangular domain and corresponding boundary conditions.

where $\dot{m}_{flow}$ is the mass flow rate in the pipe $[kg/s]$, c_f is the specific heat capacity $[J/kg \cdot K]$, T_f^k is the outlet fluid temperature $[°C]$ of each segment k, and L_{seg} is the length of the segment $[m]$.

The heat injected into each pipe inclusion cell ($q_{i,j}^{source}$), see Figure 2.6, is calculated by dividing the heat flow q_f^k into each pipe inclusion cell depending on the fluid-to-cell resistance $R_{i,j}^{pipe}$, see Paper 2. The source term $q_{i,j}^{source}$ is the thermal connection between the fluid in the pipe and the calculation cells in the HHP module according to equation 2.2. $q_{i,j}^{source}$ connects the pavement surface with the fluid inside the pipes, and the fluid can then transport heat to the thermal storage.

2.2.5 Validation of HHP-module

In order to validate the HHP module, the calculated thermal resistance between the pipe and the upper pavement surface is compared with the result obtained by an analytical solution. The thermal resistance is used because it can be calculated analytically. The validation case is schematically presented in Figure 2.7.

The analytical solution used for the validation is based on the assumption of a single pipe in an infinite pipe array placed at a depth from a surface. The HHP is considered as one example of an infinite pipe array. An analytical solution for the upward thermal resistance R_{up} is calculated according to the method described by Johan Claesson and Dunand (1983):

$$
\begin{aligned}
R_{up}^{array} &= \frac{1}{2\pi\lambda} \ln\left(\frac{cc}{2\pi d_p} \cdot \sinh\left(\frac{2\pi d_p}{cc}\right)\right) \\
R_{up}^{1,pipe} &= \frac{1}{2\pi\lambda} \ln\frac{2d_p}{r_p} \\
R_{up}^{analytical} &= R_{up}^{1,pipe} + R_{up}^{array} \quad [\frac{mK}{W}]
\end{aligned}
\tag{2.21}
$$

Table 2.1: Input data used in the validation case.

Parameter	Value	Unit
λ - Thermal conductivity (for all materials)	2.0	$[\frac{W}{m\ K}]$
cc - Centre-to-centre distance between pipes	200	$[mm]$
Domain depth	2000	$[mm]$
d_p - Depth to pipe centre	100	$[mm]$
r_p - External radius of pipe	12	[mm]
T_{pipe} - Temperature at pipe wall	1.0	$[^\circ C]$
$T_{ambient}$ - Temperature at boundaries	0.0	$[^\circ C]$

Table 2.2: Upward thermal resistance for the fine and course mesh used in the validation. The relative error is expressed with respect to the analytical result.

	Nr-cells	$R_{up}\ \left[\frac{m \cdot K}{W}\right]$	Relative error
$R_{up}^{analytical}$	-	0.3344	-
R_{up}^{HHP} - Fine mesh	154	0.3348	0.111%
R_{up}^{HHP} - Course mesh	32	0.3375	0.939%

The parameters used in equation 2.21 are presented in Table 2.1, together with the values used in the validation case. The resulting upward resistance $R_{up}^{analytical}$ is 0.3344 $[\frac{m\ K}{W}]$.

The upward thermal resistance for the HHP module is based on the temperature difference between the pipe and the ambient, and the calculated upward heat flux. R_{up}^{HHP} is calculated as

$$R_{up}^{HHP} = \frac{(T_{pipe} - T_{ambient})}{Q_{up}} \quad [\frac{m\ K}{W}] \tag{2.22}$$

where T_{pipe} is the temperature on the outside of the pipe $[^\circ C]$, $T_{ambient}$ refers to the ambient temperature $[^\circ C]$, and $[Q_{up}]$ is the heat flux passing the upper boundary $[W/m]$. The different components of equation 2.22 are presented in Figure 2.7.

R_{up}^{HHP} is calculated according to equation 2.22. The accuracy of the HHP module depends on the number of calculation cells used. By using more calculation cells, the accuracy is increased, but the computational effort also increases. The influence of the number of calculation cells is studied by comparing a course and a fine mesh. The course mesh consists of 32 calculation cells, and the fine mesh has 154 cells. The smallest possible cell size that can be used is controlled by the pipe radius, because the pipe must fit inside adjacent calculation cells (Karlsson 2010). The respective upward thermal resistances R_{up}^{FDM} for the course and fine meshes are 0.3375 and 0.3348 $[\frac{m\ K}{W}]$.

In Table 2.2, the upward thermal resistance R_{up} calculated by the HHP module is compared with the analytical solution. The relative errors are below 1% for both the fine and course meshes. Given that the course mesh should be avoided, the HHP module gives results that are deemed to be accurate. This validates that the internal heat balance of the HHP module is functioning correctly.

2.2.6 Borehole thermal energy storage module - PyGfunction

In order to prevent slipperiness on the road surface, the thermal energy harvested during the summer should be stored into the winter. Different options for seasonal thermal energy storage (STES) systems were studied in (Johnsson 2017b), and BTES systems were found to be suitable. However, the local geological conditions should be investigated and areas with certain characteristics, such as ground water flow, should be avoided. For more details on different options for STES, see (Johnsson 2017b).

The rate at which heat can be extracted from a BTES depends on three parameters, namely, the fluid temperature T_f, the temperature at the borehole wall (T_{BHW}), and the local thermal borehole resistance (R_b). R_b depends strongly on the thermal conductivity of the filling material in the borehole. Most of the boreholes in Scandinavia are groundwater-filled, owing to the geological conditions, with mostly hard crystalline rock. In contrast, other countries in Europe and America have a practice of filling boreholes with grout to protect the groundwater and to enhance the borehole resistance (O. Andersson and Gehlin 2018).

The BTES module is a modification of *Pygfunction*, which is an open-source software package based on the work by (Cimmino and Bernier 2014) and (Cimmino 2017). The software calculates fluid and borehole wall temperatures for a borehole field based on the heat load applied to the storage. The modification consists of an implementation of a routine to calculate the borehole resistance (R_b) for groundwater-filled boreholes. *Pygfunction* was modified because groundwater filled boreholes are common in Scandinavia, and the natural convection within the borehole is a challenge when determining R_b. The natural convection is a result of the temperature differences within the borehole. This natural convection reduces R_b owing to convective heat transfer. For more details on methods of calculating R_b, see Paper 3.

The boreholes modelled by the BTES module consist of a borehole drilled into the ground, equipped with a heat exchanger. The heat exchanger consists of a single U-shaped plastic tube in which a fluid is circulated to transfer heat from the bedrock surrounding the borehole (see Figure 2.8). As stated previously, boreholes are commonly filled with grout to enhance the thermal contact between the borehole heat exchanger and the borehole wall (Narsilio and Aye 2018). However, in the Scandinavian countries, the bedrock is generally of good quality and groundwater is usually close to the surface, which reduces the need for grout filling. The Scandinavian standard installation method of borehole heat exchangers starts by drilling a steel casing through the overburden and two meters into the bedrock (see Figure 2.8 (B)). Inside the steel casing, an open hole is drilled into the stable rock until the design depth is reached. Finally, the borehole heat exchanger is inserted, and a lid is mounted on top of the steel casing (O. Andersson and Gehlin 2018).

In the original *Pygfunction*, the interaction between boreholes is calculated by analytically generated thermal response factors and the borehole resistance (R_b) is determined using the multipole method based on (Claesson and Hellström 2011). In the modified software, the calculation of the borehole resistance R_b by the multipole

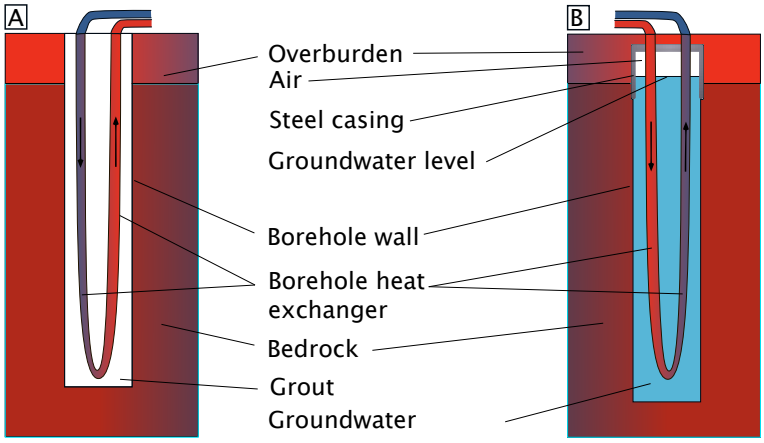

Figure 2.8: Vertical borehole with borehole heat exchanger: left (A) is a common European grout-filled borehole and right (B) is a Scandinavian groundwater-filled borehole.

method has been replaced with a method based on correlations for groundwater-filled boreholes developed by (Spitler et al. 2016). These correlations were used to find the borehole resistance R_b and the thermal resistance between the two pipes forming the U-tube, R_{12}. These resistances, Eq. 2.23 and Eq. 2.24, were implemented in *Pygfunction*.

$$R_b = R_{BHW} + \frac{R_{poc}}{2} + \frac{(R_p + R_{pic})}{2} \tag{2.23}$$

$$R_{12} = 2(R_{poc} + R_p + R_{pic}) \tag{2.24}$$

where R_p is the conductive (thermal) resistance of the pipe material and R_{pic}, R_{poc}, and R_{BHW} are the convective resistances on the inner pipe surface, outer pipe surface, and borehole wall, respectively. For more details on the implementation of the correlations for natural convection, see (Spitler et al. 2016) and Paper 3.

2.2.7 Validation of storage module

The storage module was validated against recorded data from four thermal response tests (TRTs) performed at the field station during the spring of 2018. For more details, see Paper 3. The validation was performed by running the modified Pygfunction under similar conditions as those during the TRTs, and then comparing the simulated return fluid temperatures with the observed fluid temperatures.

The borehole resistances and the return fluid temperature were calculated by three different methods. The first method used the correlations for natural convections (the modified software). The second method (unmodified Pygfunction) used the thermal conductivity of water (0.6 W/mK) as the filling material. The third method (unmodified Pygfunction) used an effective thermal conductivity of the filling material, obtained by matching the calculated return fluid temperature with respect to the measured fluid temperature. The calculated return fluid temperature was compared

Table 2.3: Comparison of measured and simulated effective borehole resistance using different settings. The values in parentheses indicate the deviation between each method and the reference method.

	TRT Para. Est.	Natural convection		Filling conductivity λ_f 0.6		Effective filling conductivity		
	$R_b^* \; m\,K/W$	$R_b^* \; m\,K/W$	ME $°C$	$R_b^* \; m\,K/W$	ME $°C$	k_g	$R_b^* \; m\,K/W$	ME $°C$
TRT1	0.105 (ref)	0.123 (17%)	0.432	0.143 (36%)	0.862	1.2	0.102 (−3%)	−0.013
TRT2	0.086 (ref)	0.112 (31%)	1.027	0.143 (67%)	2.588	1.7	0.090 (5%)	−0.047
TRT3	0.094 (ref)	0.108 (15%)	1.461	0.143 (52%)	4.005	1.8	0.089 (−6%)	0.004
TRT4	0.084 (ref)	0.088 (5%)	0.776	0.134 (60%)	3.659	2.0	0.073 (−13%)	0.041

to the measured return fluid temperature of the TRTs and the mean error (ME) was calculated. Furthermore, the results of these three methods were compared to the effective borehole resistance obtained by the parameter estimation method of the TRTs. The results of the comparison are presented in Table 2.3.

The constant thermal conductivity of the filling material (0.6 W/mK) results in significant differences, compared to the reference method, both for the effective borehole resistance (R_b^*) and the return fluid temperature. A positive ME value indicates that the return fluid temperature is overestimated. The calculated effective borehole resistance deviates between 36% and 67%, indicating that natural convection plays a major role in the heat transfer in a groundwater-filled borehole. Furthermore, the influence of the natural convection on the borehole resistance is evident by comparing the calculated R_b^* with a fixed thermal conductivity of the filling material (0.6 W/mK) and effective filling conductivity. The results reveal that the effective thermal conductivity should be in the range of 1.2 to 2 W/mK in order to calculate an R_b^* similar to the parameter estimation. This is approximately two to three times higher than the thermal conductivity of water, indicating the large influence of natural convection in the boreholes.

By using an effective conductivity for the filling material, the modified software provides similar results for the borehole resistance as the resistances obtained by the TRT, with a deviation of less than 13%. Comparing the mean error of the matched fluid temperature and the measured fluid temperature indicates an agreement of approximately ± 0.05 $°C$, which is considered to be a good agreement.

Finally, when comparing the borehole resistance taking natural convection into account with the borehole resistance from the TRTs, there is a general overestimation of the effective borehole resistance. The overestimation is in line with that reported by (Spitler et al. 2016). There is good match for TRT4, with a deviation of ± 5%. However, TRT1, TRT2, and TRT3 reveal a much larger deviation on both the borehole resistance and the mean error of the fluid temperature. The large deviation in R_b^* of approximately 15% to 30% is a challenge that requires further research. However, when comparing our results to those reported by (Spitler et al. 2016), the deviations are within the range of what they found in their study. This indicates that the modified Pygfunction can be used to simulate shallow geothermal systems with groundwater-filled boreholes.

2.3 Parameter influence on harvesting potential

The influence of different parameters on the harvesting potential has been studied previously. Nasir et al. 2016 studied the influence of the pipe diameter, fluid velocity, pipe depth, and inlet water temperature. They found that, in order to obtain a large temperature difference of the fluid in the pipe, the PSC should be designed with a small pipe diameter, shallow pipe depth, low fluid velocity, and low inlet fluid temperature.

In Paper 4, the influences of the solar absorptivity, fluid flow rate, and pipe spacing on the amount of harvested energy were investigated. The influences were investigated by studying the absolute amount of harvested energy, but also by the relative measurement of PSC efficiency, η_{PSC}^{day}. The PSC efficiency is calculated according to

$$\eta_{PSC}^{day} = \frac{\sum_{t=1}^{day} Q_{PSC}}{\sum_{t=1}^{day} q_{sw} \cdot A_{PSC}} \tag{2.25}$$

where Q_{PSC} is the energy flow from the pavement for each hour and $q_{sw}A_{PSC}$ is the amount of incoming solar energy falling on the pavement surface. η_{PSC}^{day} is defined on a daily basis in order to provide a measurement with a reduced influence of the large thermal mass of the PSC.

2.3.1 Influence of albedo

The potential of absorbing solar energy by a surface depends strongly on the albedo of the surface. Albedo is not constant, and the albedo of pavement surfaces is usually subject to time-dependent variation. Bitumen-based materials usually become lighter owing to ageing of the bitumen and wear, whereas concrete pavement tends to become darker owing to particles from traffic bonding to the surface (U.S Environmental Protection Agency 2012). The albedo of concrete pavements commonly varies between 0.4 and 0.25, whereas that of asphalt pavements varies from 0.05 to 0.20 (U.S Environmental Protection Agency 2012; Jansson et al. 2006; Li et al. 2013; Chen et al. 2019).

The amount of energy absorbed by a concrete surface with an albedo of 0.05 to 0.4 was calculated using HyRoSim. The weather data and control settings were the same as those used at the field station during the summer of 2018. The results indicate that by changing the albedo of a surface from 0.4 (0 %) to 0.05 (-88%), the amount of harvested energy can be increased from approximately 240 to 320 kWh/m^2, i.e. an increase of approximately 30% (see Figure 2.9).

2.3.2 Influence of fluid flow

The fluid flow rate affects the amount of energy that can be harvested. A higher fluid flow rate results in a lower mean temperature of the fluid, which increases the heat transfer. If the flow rate is too low, the PSC is not efficiently used, because the temperature difference between the fluid and pavement is low. A higher flow rate

gives a larger temperature difference between the pavement surface and the fluid, which increases the amount of harvested energy and reduces the mean pavement temperature. An increase in the fluid flow from 0.02 to 0.17 l/s (−75% to 50% relative to the settings used during the summer of 2018) leads to an increase in the harvested energy from 140 to 280 kWh/m^2 (see Figure 2.9). However, an increase in the fluid flow means an increase in the electrical energy required by the pumps. Thus, the fluid flow rate should be optimised.

2.3.3 Influence of pipe distance

The position of the embedded pipes in the pavement has a major influence on the amount of energy collected. Generally, a shallower pipe position and a shorter distance between pipes leads to a higher amount of harvested energy. Periodic maintenance activities of a pavement restrict the shallowest position of a pipe system to a depth of 5 to 7 cm below the surface of the pavement. However, the distance between two adjacent pipes (cc) can be reduced. The influence of pipe spacing was investigated by calculating the harvested energy for distances of 5 to 15 cm between the pipes. The results of the calculation are presented in Figure 2.9.

The calculated amounts of energy harvested for pipe spacings of 5 cm (0%) and 15 cm (200%) were 250 and 120 kWh/m^2, respectively, i.e. a shorter pipe distance by a factor of three leads to larger energy harvest by 108%. However, there are other limiting factors when placing the pipes close to each other. For instance, the bending radius of the pipes cannot be too short, because there is a risk of damaging the pipes. Furthermore, the load-bearing capacity of the pavement might be reduced if there are too many pipes embedded in the pavement.

2.3.4 Parameter sensitivity

The influences of each of the three investigated parameters were combined and the daily efficiency (η_{PSC}^{day}) was calculated. The reference system refers to the parameter values used during the experiments of summer 2018. By decreasing the albedo, the efficiency was increased from 42% (reference system) to 49% (see Figure 2.9). However, this required a reduction in the albedo by 50%. Increasing the pipe spacing by 50% led to a reduction in the efficiency to 34 % (from 42%). A 50% increase in the fluid flow would yield an efficiency of 49%.

The efficiency of the system can be increased to 49% (from 42%) by either making a 50% change to the fluid flow rate or the albedo. Comparing the efficiency of the PSC presented in Figure 2.9 with previously reported efficiencies of 30% (Loomans et al. 2003) and 15% to 20 % (Guldentops et al. 2016), it is clear the efficiency reported in this study is above those of previous studies. One reason for this may be that Guldentops et al. uses a pipe spacing of 15 cm, which is twice that in this study. Furthermore, a much lower flow rate was used by Guldenstops. Loomans et al. used a spacing of 15 cm, but with an albedo of 0.2 and a lower supply temperature of 10 $°C$, which results in a higher efficiency. It can be concluded that the simulations and measurement from this study are in line with previously reported results.

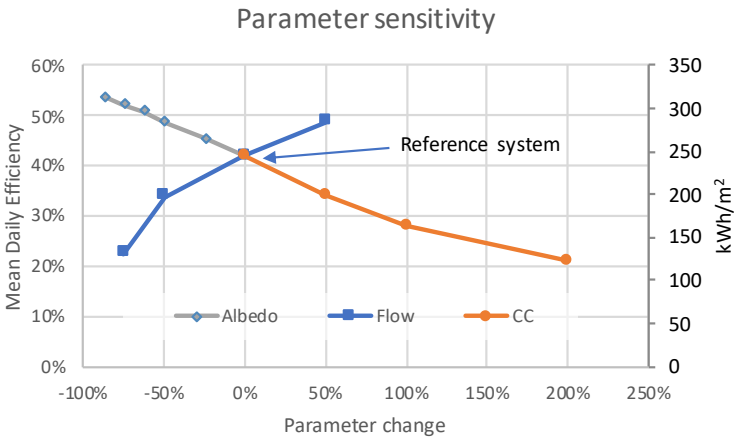

Figure 2.9: Calculated mean value of the daily efficiency for different variations of fluid flow, albedo, and pipe spacing.

2.4 Influence of dew point regulation on energy demand

Paper 2 investigated the influence of two different control strategies for an HHP system. One of these strategies takes only the air temperature into account and the other also takes the dew point temperature into account. The dew point is important, because in order to have condensation and ice formation, the following condition must hold: $T_{surface} < T_{dew} \quad \& \quad T_{surface} < 0°C$.

By maintaining the surface temperature above the dew point temperature, condensation can be avoided, which prevents ice formation. This control strategy can be used to reduce the energy demand of HHP systems and was discussed in Johnsson (2017).

The two strategies used the same snow ploughing settings and supply temperatures. Snow was removed from the surface when the snow cover exceeded 1, 3, or 200 cm. The snow ploughing initiations levels were selected to represent a road with high, medium, and no snow ploughing. By using an initiation level of 200 cm (no ploughing, as the snow level never exceeds 200 cm), it is possible to investigate function of the HHP system independently of snow ploughing. The supply temperature was varied between 2 and 8 $°C$.

The basic air temperature regulation was designed to start the HHP system when the air temperature drops below 1 $°C$ and stop the system when the air temperature goes below -6 $°C$ in order to conserve energy. The system can be stopped owing to the lower likelihood of precipitation and the slow rate of frost formation at low temperatures (Knollhoff et al. 2003).

The dew point regulation was designed based on weather forecasts. The heating is started 6 h before the surface temperature drops below the dew point temperature and before any precipitation reaches the pavement surface. Given that the air temperature is above -6 $°C$, the HHP system is started if the surface temperature is

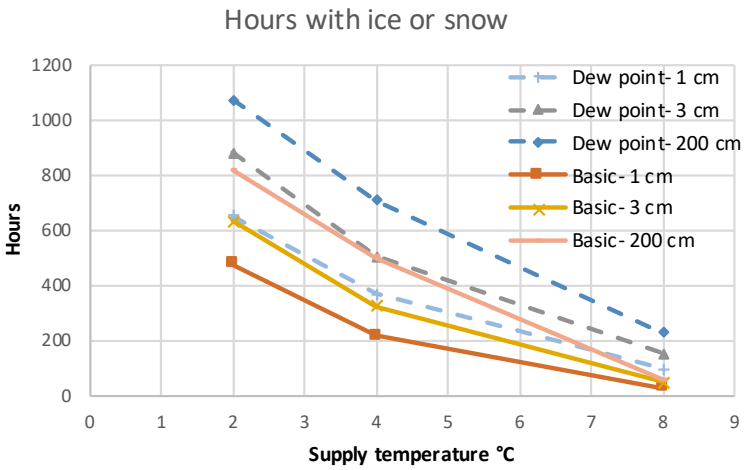

Figure 2.10: Number of hours with ice- and snow-covered road surface, at different supply temperatures, snow removal strategies, and control strategies: basic and dew point.

lower than the forecasted dew point temperature or if the weather forecast predicts snowfall.

The number of hours with snow and ice on the pavement is strongly affected by the HHP system (see Figure 2.10). Without heating, there are approximately 1,800 h with snow or ice on the pavement. However, under the basic regulation, the ice and snow cover last for only 480 h when using a supply temperature of 2 $°C$ and snow ploughing when the snow cover is thicker than 1 cm. There is a clear difference between the two control strategies. The dew point regulation generally performs worse when considering the number of hours with snow on the pavement. The number of hours with snow and ice on the pavement is 650 h compared to 480 h when using a snow ploughing initiation level of 1 cm. The reason for this is that during strong cold spells, the time to heat up the pavement surface might be longer than the available 6 h. However, the benefit of using the dew point regulation is the strong reduction in the energy demand.

The dew point regulation reduces the time during which the HHP system is active, which significantly reduces the energy demand (see Figure 2.11). The energy demand is only 125 kWh/m^2, compared with 330 kWh/m^2 for the air temperature regulation. This represents a 62% reduction in the energy demand. From Figure 2.11, it is evident that there is a large potential to reduce the energy demand of an HHP system by using dew point regulation, and the difference increases with higher supply temperatures.

The snow ploughing initiation level only has a small influence on the energy demand (see Figure 2.11). This is because there is a limited number of hours with snowfall compared to the risk of frost formation. However, the initiation level is important for the surface conditions (see Figure 2.10). This is especially important when the available heating power is limited, i.e. when the supply temperature is low. For a higher supply temperature, the available power is sufficient to melt the snow

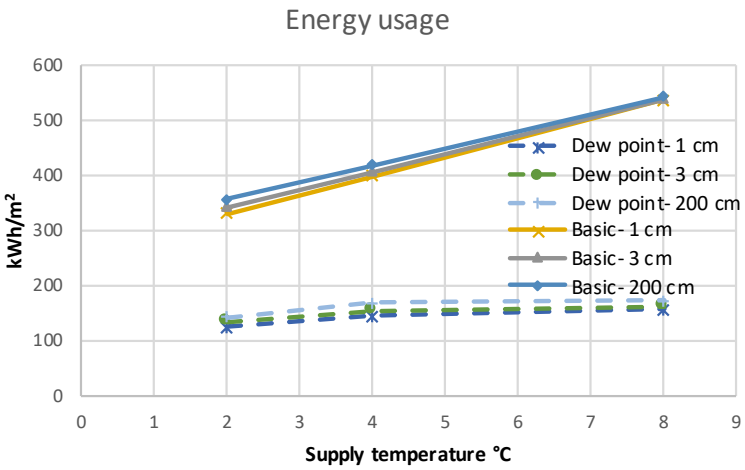

Figure 2.11: Energy usage for winter maintenance for different supply temperatures, snow removal strategies, and using two different control strategies: basic and dew point.

and ice away.

The control system plays an important part with respect to reducing the energy demand. The control system is more important than the snow removal strategies, particularly for higher supply temperatures.

Chapter 3

Experimental studies

The experimental parts of this thesis build on results from an HHP field station. However, before any experiments on the HHP could commence, the thermal properties of the pavement materials, the working fluid, and the ground were measured. This chapter describes these measurements and presents a general overview of the field station.

3.1 Field station

In 2017, a field station for HHPs was constructed outside Östersund (63.18 N, 14.5 E) in Sweden. The field station is part of a Nordfou project named HERO (Heating Road with Stored Solar Energy), the major funders of which are the public road administrations of Sweden, Norway, and Finland. The aim of the field station is to investigate and demonstrate the concept of using HHPs with stored solar energy. The HHP will be used for preventing slippery road conditions in the winter and as a PSC in the summer. The information from the field station will be used for the verification of a numerical model and to acquire general experience with the technique.

The main challenges are set by the harsh Scandinavian climate, with its long winters. The climate imposes special demands on how to utilise the limited energy that has been harvested. This will be handled by using a low-temperature system working with supply temperatures below 10 $^{\circ}C$.

Figure 3.1 gives a general overview of the field station. The field station consists of five major components, namely a weather station, service building, BTES, hydronic heated surface, and reference surface. The heated surface is made from concrete and contains plastic pipes that transfer heat to the pavement. The reference surface is used for a comparison to see the effect of the HHP. The energy used by the system is extracted from the BTES, which consists of four boreholes that were drilled with an equal spacing of 10 m to a depth of 210 m. According to previous geological surveys, the boreholes were drilled in clay slate covered by approximately 10 m of glacial till. TRTs were performed in May 2018 and the ground thermal conductivity was determined as 3.15 W/mK, with a thermal capacity of 2.8 MJ/m^3K (Johnsson

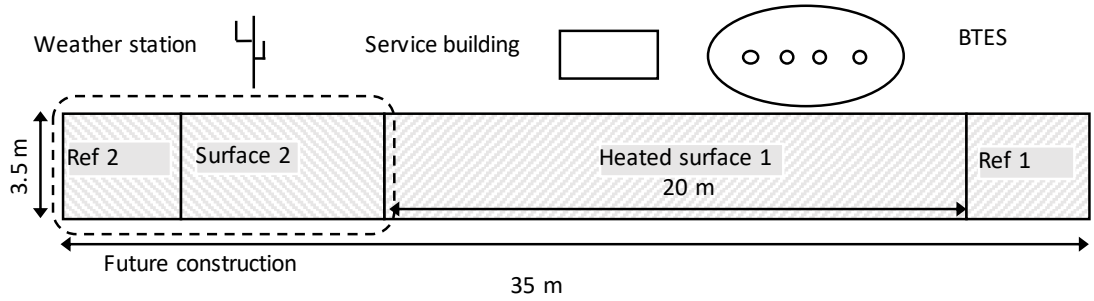

Figure 3.1: Main components and layout of the field station in Östersund.

(a) Pipe in the HHP. (b) Mounting temperature sensors

Figure 3.2: HHP before casting the concrete pavement.

and Adl-Zarrabi 2019). Each borehole contains a single 40×2.4 mm U-tube thermal collector.

The service building holds all the measuring equipment and pumps required for the system. In the service building, there is also an electric boiler as a backup. The weather station provides information on the local weather (air temperature, relative humidity (RH), wind, precipitation, camera), which is used for both controlling the system and evaluating the measured results.

The heated surface was constructed with a top layer of concrete that contains a pipe placed at a depth of 62 mm (pipe centre) and with a spacing of 50 mm (see Figure 3.3b). Underneath the top layer, the HHP was prepared as a regular road, but with an insulation layer that gave more stable boundary conditions and reduced the risk of frost heave. The pipes are made of cross-linked polyethylene with the dimensions of 20×2 mm^2. Ten parallel pipes go back and forth in the concrete, giving a total length of approximately 140 m and covering an area of 70 m^2 (see Figure 3.2a).

The field station is monitored by many sensors and the temperature distribution in the pavement and along the pipes is measured by four-wired PT100 resistance temperature detectors (Pentronic 7912000 PT100 1/5 DIN, see Figure 3.3a). PT100 sensors were selected because of their good long-term stability, as well as their common utilisation in road applications. In each measuring section, the surface and pipe outer surface temperatures (T1 and T3, respectively) are measured. In Figure

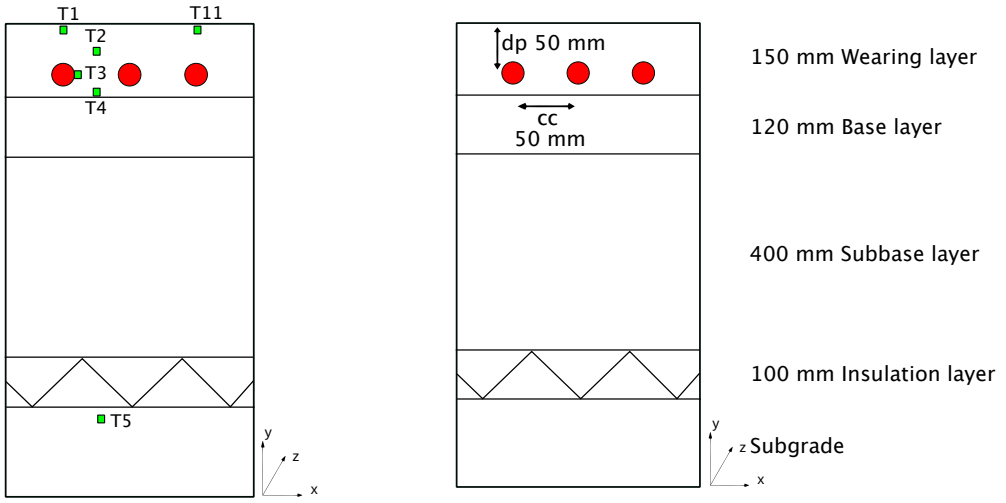

(a) T1: 5 mm, T2: 30 mm, T3: 50 mm, T4: 150 mm below the pavement surface.

(b) Pipe placement and thickness of pavement layers.

Figure 3.3: Design of the pavement with sensors and layers in the field station.

Table 3.1: General input parameters for the studied PSC system. Fluid properties at 5 $°C$.

Parameter	Value	Unit
Fluid flow in one pipe	0.114	l/s
Distance between the pipes	50	mm
Embedded depth (from centre of the pipe to the surface)	62	mm
Length of pipe	140	m
Surface emissivity (dry, moist, wet, frost, ice, snow)	0.80, 0.85, 0.9, 0.97, 0.97, 0.9	-
Surface albedo (dry, moist, wet, frost, ice, snow)	0.4, 0.25, 0.2, 0.5, 0.5, 0.9	-
Density of fluid	1070	kg/m^3
Specific heat capacity of fluid	3258	J/(kg·K)
Thermal conductivity of fluid	0.389	W/(m·K)
Dynamic viscosity	5.88	mPa·s
AADT-Annual average daily traffic	12	-
Pump power	500	W

3.2b, the temperature sensors in a measuring section are positioned before casting the concrete.

The fluid flows and temperatures are monitored in the service building. The fluid temperature is measured with PT100 sensors at multiple points (see Figure 3.4). Based on the measured temperatures and fluid flow, the heat flows can be calculated for the pavement, storage, and boiler.

A complete overview with drawings can be found in (Sundberg 2019).

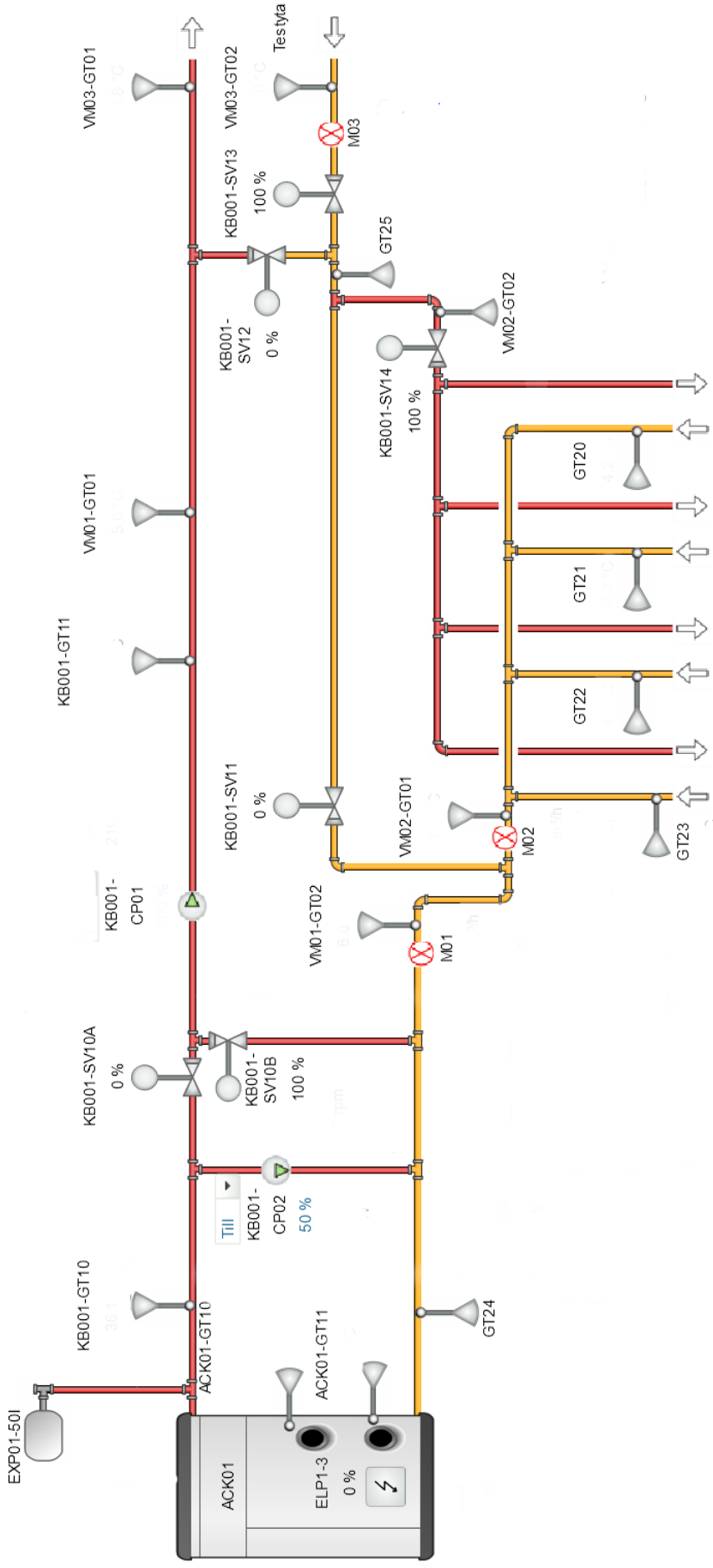

Figure 3.4: System layout.

Table 3.2: Properties of the construction materials.

Layer	Thickness $[mm]$	Material	Density $[kg/m^3]$	C_p $[J/kg \cdot K]$	λ $[W/mK]$	$\lambda_{measured}$ $[W/mK]$
Wearing layer	150	Concrete C35/45	2200	900	2.1	2.1
Pipes	20	PE-Xa 20x2 mm	925	2300	0.35	-
Base layer	120	Gravel 0–40 mm	2030	900	0.6	0.28
Subbase layer	400	Gravel 0–80 mm	2000	900	0.8	0.27
Insulation	100	XPS 500	30	1200	0.035	-
Subgrade layer	5000	Glacial Till	1800	900	1.2	0.41

3.2 Thermal properties

3.2.1 Pavement materials

The HHP consists of different layers, according to Figure 3.3b. Each of these layers has different thermal properties that need to be determined. However, the laboratory conditions differ from the conditions within the road construction. Therefore, it is a challenge to determine the true thermal conductivity (λ), specific heat capacity (C_p), and density (ρ) of the materials. The thermal properties depend on the aggregates, moisture content, and grade of compaction. Given the available facilities, it was not possible to correctly measure the thermal conductivity of the unbound materials, as can be seen in Table 3.2 and $\lambda_{measured}$. For the unbound materials of the base, subbase, and subgrade layers, the guarded hot plate method was used to measure the thermal conductivity. However, the grade of compaction obtained was not sufficient to represent real conditions and the resulting thermal conductivity ($\lambda_{measured}$) was two to three times lower than the expected value (λ). Therefore, values found in the literature have been used (λ) (Nuijten 2016). The thermal conductivity of the wearing layer was measured using the transient plane source method, which is suitable for bound materials such as concrete and asphalt concrete (Mirzanamadi et al. 2018).

3.2.2 Determining fluid properties

The fluid in the pipes of the HHP is an ethylene glycol solution, which was specified to consist of a 45% Dowcal solution. However, the fluid properties were identified as a main contributor to the measurement uncertainty of the heat flows. To verify the concentration, experiments were performed to investigate the freezing temperature of the fluid. Based on the freezing temperature, the thermal properties can be estimated from tabulated values (Melinder 2007).

The experiment was performed by placing a 12-ml sample inside a climate chamber (see Figure 3.5). While monitoring the temperature inside the sample and in the ambient air in the climate chamber, the temperature in the climate chamber was cycled between -25 and -40 $^\circ C$. The freezing temperature was identified by studying the temperature curve of the sample and identifying the level at which the temperature stabilises. The experiment was repeated 20 times and the likely freezing

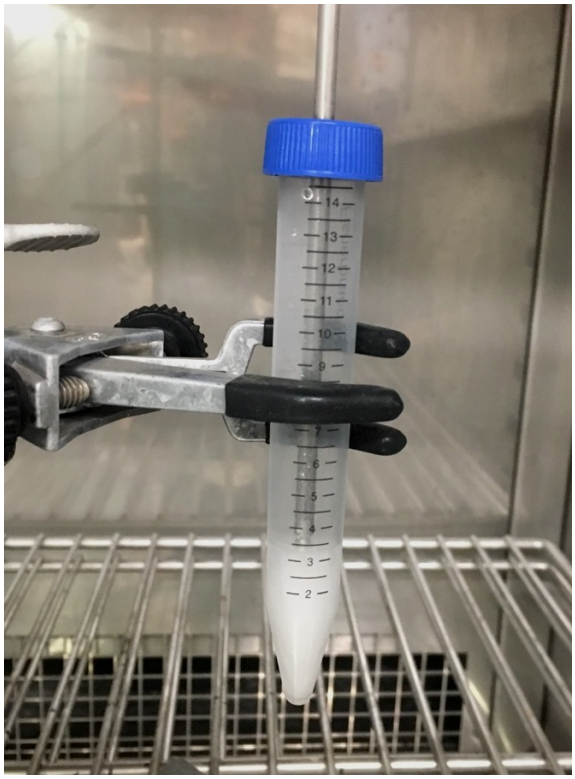

Figure 3.5: Partly frozen fluid sample during freeze testing. The vertical metal rod inside the sample is the thermometer.

temperature was estimated to be $-32\ ^{\circ}C$, which corresponds to a concentration of 47%. The resulting fluid properties can be seen in Table 3.1.

3.2.3 Thermal response test

A common method to estimate the ground thermal conductivity (λ) and effective borehole resistance (R_b^*) is to use TRTs. These two parameters are important for designing BTES systems, and also for simulating the performance of an HHP connected to a BTES. In Paper 3, the results from TRTs are evaluated based on the simplified line-source theorem.

The TRTs were performed by injecting a constant heat load into the borehole heat exchanger, and at the same time monitoring heat injection rate, fluid flows, and fluid temperatures. By evaluating how the fluid temperature develops over time in relation to the heat injection rate, the thermal conductivity of the ground (λ) can be estimated (Gehlin 2002).

In Paper 3, the ground thermal conductivity was determined by evaluation of the TRTs using two methods, the simplified line-source theorem and parameter estimations. The estimated thermal conductivity was compared to identify the variation between the evaluation methods. The mean value of the thermal conductivity obtained from the two methods was used in the modified software for calculations of borehole fluid temperatures.

The method used is based on a linearisation of the simplified line-source theorem. The mean fluid temperature (T_f) over time can be calculated by using Eq. 3.1, according to (Gehlin 2002).

$$T_f(t) = T_g + \frac{q}{4\pi\lambda}\ln(t) + q\left[\frac{1}{4\pi\lambda}\left(\ln\left(\frac{4a}{r_b^2}\right) - \gamma\right) + R_b^*\right] \tag{3.1}$$

where q is the heat injection rate, λ is the thermal conductivity of the ground, t is the time, a is the thermal diffusivity calculated as $a = \frac{\lambda}{\rho\, c_p}$, ρ is the density of the ground, c_p is the specific heat capacity, r_b is the diameter of the borehole, γ is Euler's constant (0.57772), R_b^* is the effective borehole resistance, and T_g is the undisturbed ground temperature. The linear Eq. 3.1 can be rewritten as Eq. 3.2.

$$\begin{aligned} T_f(t) &= K \cdot \ln(t) + m \\ K &= \frac{q}{4\pi\lambda} \\ m &= q\left[\frac{1}{4\pi\lambda}\left(\ln\left(\frac{4a}{r_b^2}\right) - \gamma\right) + R_b^*\right] + T_g \end{aligned} \tag{3.2}$$

where K and m can be obtained by fitting a linear function to the observed mean fluid temperature plotted versus the time logarithm. With a known heat injection rate q, the thermal conductivity λ of the ground and effective borehole resistance R_b^* can be estimated. For more details, see (Gehlin 2002).

An alternative method for evaluating TRTs is parameter estimations of the line-source theorem. This method is based on a numerical optimisation of the parameter values, λ and R_b^*, in Eq. 3.3 that provide the best match with the observed temperature curve from the TRT. The matching is done by minimising the sum of the squared errors (Gehlin and Hellstrom 2003). This method has the benefits of being more accurate than the simplified line-source method when the heat injection has small variations.

$$T_f(t) = T_g + \frac{q}{4\pi\lambda}E_1\left(\frac{r_b^2}{4at}\right) + qR_b^* \tag{3.3}$$

where E_1 is the exponential integral and the other parameters are the same as in Eq. 3.1.

Four different thermal response tests (TRT1–TRT4) were performed and evaluated using the two methods. Table 3.3 presents the heat loads and volumetric flows used during the TRTs and the resulting thermal conductivities and borehole resistances. In the analysis, the first 14 h of the test have been removed in order to only study the part of the TRT representing the steady-state heat flux. The results reveal variations in both the ground thermal conductivity and the effective borehole thermal resistance. The variation was expected, as the TRTs were performed on individual boreholes, which were subjected to different loading conditions and possibly varying geological situations. The mean thermal conductivity estimated by the simplified line-source approximation and the parameter estimations showed similar results of 3.16 and 3.15

Table 3.3: Results from TRT performed at the test site. Values in parentheses are deviations from the mean value. TRT1 was performed on four boreholes with the depth of 200 m.

	Borehole L m	Load W/m	Flow in U-tube m^3/h	λ: line-source W/mK	λ: parameter esti. W/mK	R_b^*: line-source $K\,m/W$	R_b^*: param. esti. $K\,m/W$
TRT1	4×200	22	1.598	3.342 (6%)	3.340 (6%)	0.105	0.105
TRT2	200	47	1.524	2.727 (−14%)	2.703 (−14%)	0.087	0.086
TRT3	200	70	1.442	2.975 (−6%)	2.963 (−6%)	0.093	0.094
TRT4	200	50	2.285	3.589 (14%)	3.588 (14%)	0.084	0.084
			Mean	3.158	3.149		

W/mK. The result of each TRT (TRT1–TRT4) revealed small variations between the evaluation methods. The variations observed in the results of this study are in the 10% uncertainty range reported from TRT, and within the 7% variation between adjacent boreholes that has been reported in other studies (Javed et al. 2011). The effective borehole resistance (R_b^*) reveals a small variation between the two methods.

Based on the TRTs, the average thermal conductivity of the ground is calculated to be 3.15 W/mK.

Chapter 4

Concept validation

An HHP system should be able to harvest solar energy during the summer and store the energy until the winter, when the energy should be used for WRM. This concept for an HHP system was evaluated during the summer of 2018 and winter of 2018/2019. The result from these tests are presented in this chapter. The numerical simulations by HyRoSim used the input data in Table 3.1 and geometrical dimensions and thermal properties given in Table 3.2. Furthermore, HyRoSim requires weather data on air temperature, RH, wind speed, global radiation, cloudiness, and precipitation. The weather data were measured at the field station, except for the cloudiness and global radiation. The cloudiness was collected from weather forecast by the Swedish Meteorological and Hydrological Institute and the global radiation was measured at a weather station 10 km from the field station.

4.1 Harvesting 2018

The amount of solar energy that can be harvested from the pavement sets a limit on how much energy could be used by the HHP system, and this was studied in Paper 4. The HHP system should not consume more than the energy available in the thermal storage. To find out how much energy could be harvested, measurements were performed at the field station during the summer of 2018. The measurements started on the 14^{th} of May and ended on the 31^{st} of August. The summer of 2018 was exceptionally warm, with a mean air temperature 2 $°C$ above average, which increased the amount of harvested energy. During the summer, the accumulated energy (E_{PSC}) from the PSC and the heat extraction rate (Q_{PSC}) were measured (see Figure 4.1). The heat extraction rate reached peak values of 20 kW, and the daily mean varied between 4 and 10 kW. The total accumulated energy during the period was 17,200 kWh, which is equivalent to 245 kWh/m^2, and the total amount of incoming solar radiation was 614 kWh/m^2.

The solar efficiency of the PSC during the summer of 2018, calculated according to Equation 2.25, was found to be 42%. This is higher than the efficiencies reported in other studies (Loomans et al. 2003). The higher efficiency of the field station in Sweden can be explained by a shorter pipe distance of 5 cm, high fluid flow rate, and low supply temperature, all of which are factors that increase the solar efficiency.

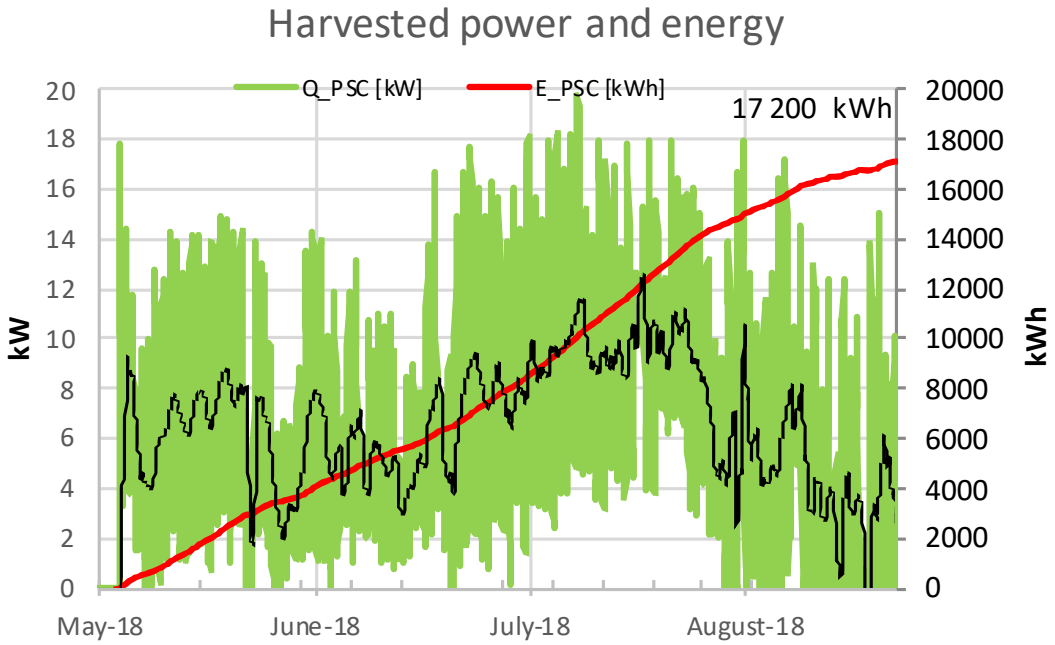

Figure 4.1: Power and accumulated energy flow from the PSC during the summer of 2018. The black line is the daily mean heat harvest rate.

The harvested energy resulted in a reduction in the pavement surface temperature, which could potentially increase the lifetime of the pavement. The mean temperature reduction during the summer was 6.4 $°C$, in comparison with the reference surface, and a maximum reduction of 10 $°C$ was recorded during the month of July (see Figure 4.2). This temperature reduction increases the service life of the pavement and for some structures, the lifetime can be increased by 50% (Ebrahim Abu El-Maaty 2018).

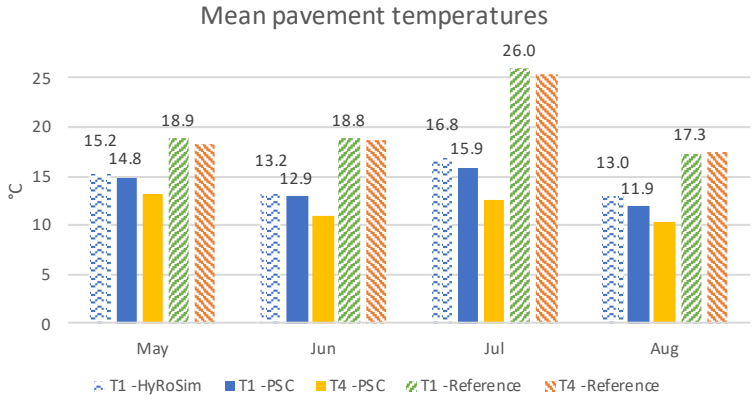

Figure 4.2: Daily mean pavement temperatures during the summer of 2018. T1-PSC refers to the PSC surface temperature (5 mm), T4-PSC is located at the bottom of the wearing layer (150 mm). 'Reference' refers to the reference surface.

The fluid temperatures, surface temperatures, and energy harvested by the PSC

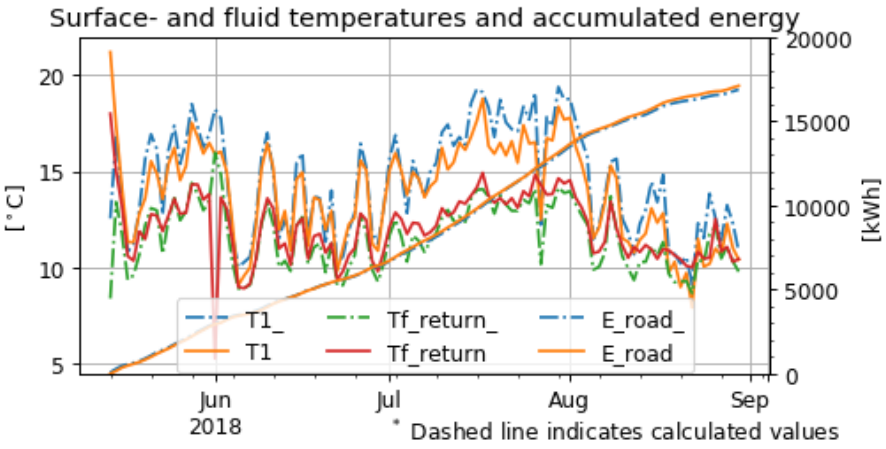

Figure 4.3: Daily mean values of calculated and measured surface temperature, return fluid temperature, and harvested energy.

were calculated by using the developed software, HyRoSim, and the results of the calculations were compared to the measured results obtained at the field station.

Figure 4.3 shows the daily mean values for the surface temperature, return fluid temperature, and accumulated harvested energy. The accumulated energy calculated by HyRoSim was equal to 16,962 kWh, which was in good agreement, with a difference of the order of 1%, with the accumulated energy measured from the field station, 17,200 kWh.

The calculated surface temperature was 2% to 8% higher than the measured surface temperature (see Figure 4.2). The deviation between the calculated and measured results depends on the spatial uncertainty of the embedded temperature sensor in the pavement. There might be a difference between the design position and the real position after casting the pavement. Considering this spatial uncertainty, the absolute pavement temperature can be assumed to be accurate, with a mean deviation of 0.65 $°C$. Furthermore, the mean absolute deviation of the return fluid temperature was -0.54 $°C$.

4.1.1 Surface condensation due to harvesting

The lower surface temperature can cause condensation of moisture on the surface of the pavement if the surface temperature is lower than the dew point temperature of the ambient air. During the summer of 2018, the conditions for condensation were observed for approximately 400 h. Photographs taken by the monitoring system at the test site confirm surface condensation at a number of these hours (see the darker colour of the PSC in Figure 4.4). Surface condensation on the PSC has not been reported before. However, it might pose a risk if sudden temperature changes (below or equal to 0 °C) of the ambient air cause ice formation at the surface. However, during the measurement period, the temperatures were well above the freezing temperature, which prevented risk of ice formation. Furthermore, the condensation of moisture releases latent heat that might stabilise the temperature of the pavement during night-time. However, the same amount of energy will be

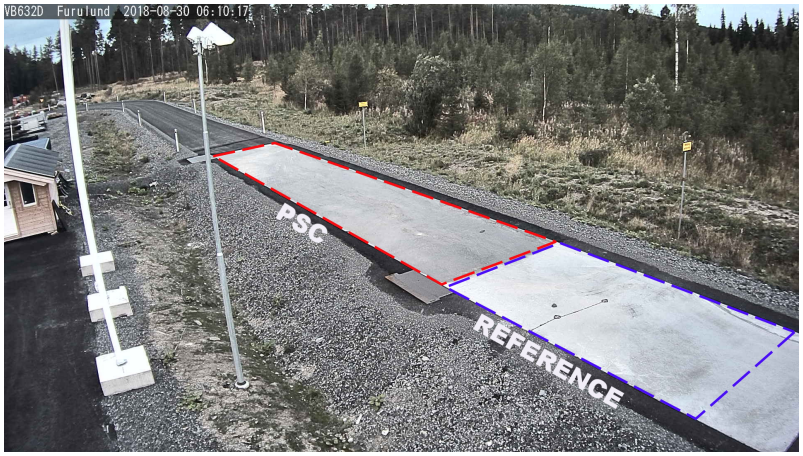

Figure 4.4: Condensation of water due to low temperatures on the PSC surface. Darker colour on the PSC surface indicates moisture.

needed for evaporation. Therefore, the net addition of latent heat from condensation and evaporation should be zero.

4.2 Winter 2019

The HHP system was tested during the winter of 2018/2019 in order to determine the energy usage of the HHP system and how the HHP would affect the surface conditions. The experiments were conducted between the 15^{th} of October 2018 and the 10^{th} of April 2019. Some of the measurements from the period are presented in Figure 4.5 as daily mean values. The mean air temperature were -3.5 $°C$ with a standard deviation of 6.5 $°C$ and the lowest recorded temperature were -24.6 $°C$, see Figure 4.5 (b). During the winter there were about 70 days with snowfall and the test surface were ploughed at 8 occasions, see Figure 4.5(a).

The HHP system used 133 kWh/m^2 of heat during the winter of 2019, see Figure 4.5 (e). The energy originates from two different sources, namely the BTES and the electric boiler. In Figure 4.6, the heat delivered from the storage and the heat supplied to the pavement can be seen, as well as the accumulated energy supplied to the road from the electric boiler and the BTES. The energy supplied to the road reached 9,356 kWh (133 kWh/m^2) and the energy delivered from the storage was 4,358 kWh (62 kWh/m^2).

The difference between the amount of heat supplied to the pavement and the heat extracted from the BTES is the energy that comes from the boiler and heat from the pumps. The electric energy used during the winter were 4,613 kWh (66 kWh/m^2). About 50 % of the energy used origins from electricity because of the need for higher supply temperatures to the pavement than the BTES could deliver. The need for electric energy were anticipated due to the cold weather in Östersund. However, the energy measured from the boiler and the storage do not add up to 133 kWh/m^2 (62+66=128). This represents an error of about 4 % that is due to the uncertainty of the energy measurements. The error can be related to the uncertainty

of the flow meters, temperature sensors and fluid properties.

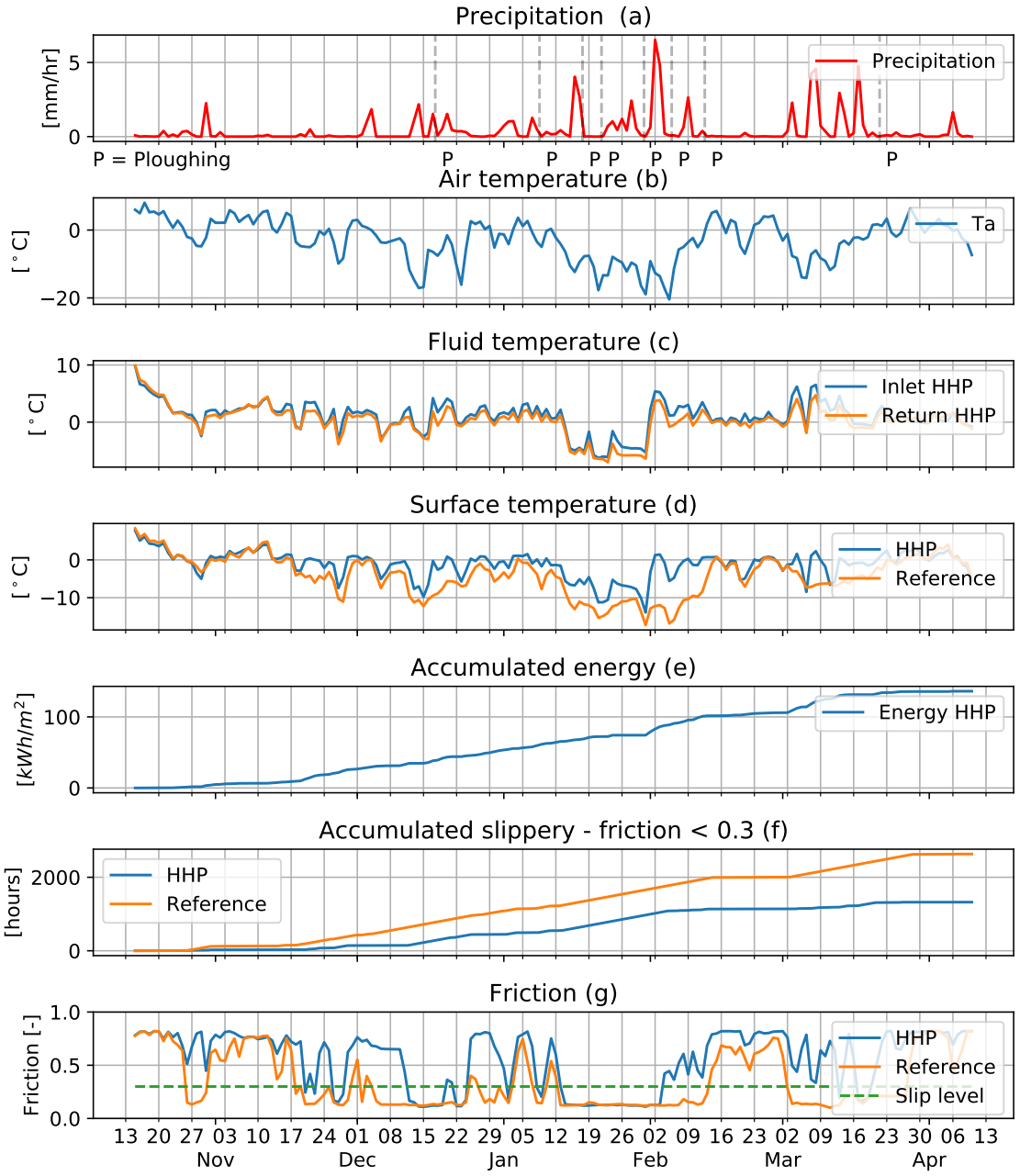

Figure 4.5: Daily mean values during the winter of 2019.

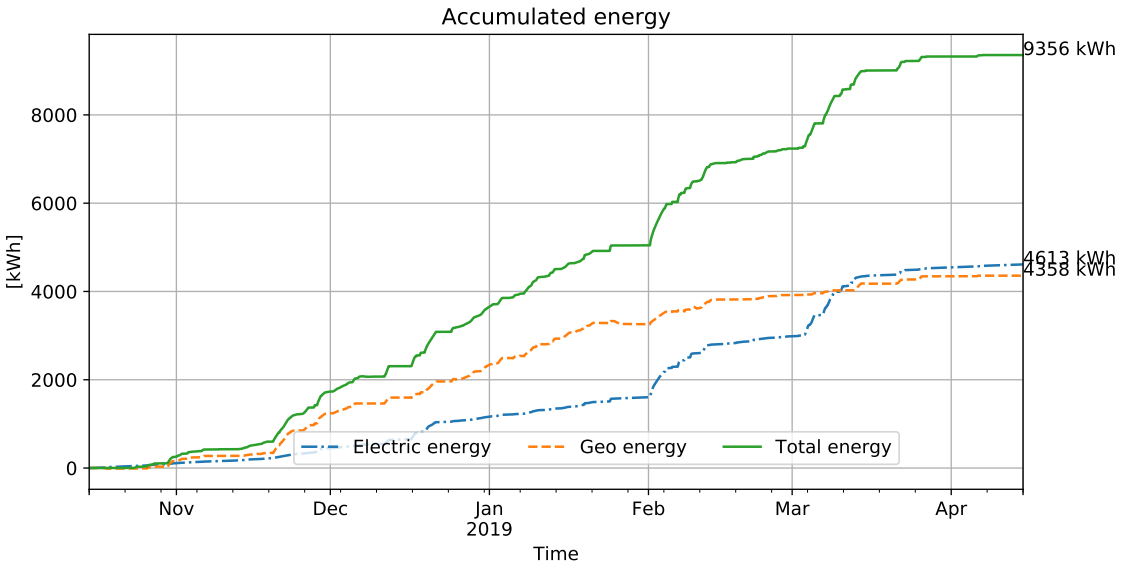

Figure 4.6: Energy demand and energy sources for the winter of 2018/2019.

4.2.1 Surface conditions

The HHP system affects the surface conditions by increasing the temperature, which melts snow and ice on the pavement. The effect on the surface conditions was studied by comparing the number of hours with risk of frost, and when the measurements indicated low friction on the reference and test surface. The hours with risk for frost were calculated based on the following requirement: $T_{surface} < T_{dew} \quad \& \quad T_{surface} < 0°C$ in a similar way as (Mirzanamadi 2019). Furthermore, the conditions were also considered to be slippery when the friction measurements were below 0.3. When considering the number of hours with risk for condensation and frost, the reference surface had 1340 h with risk for frost, and the test surface only had 230 h.

The observed friction levels are shown in Figure 4.7. The measurements were performed by two remote surface state sensors from Vaisala (DSC111). 'HHP surface' refers to the test surface and 'Reference surface' refers to the unheated surface. In general, the test surface performed much better; however, in mid December and late January, the system could not maintain the friction. This was due to a computer failure and cold weather, with air temperatures approaching $-20\ °C$. Figure 4.5 (f) shows the accumulated hours with slippery road conditions. The accumulated slippery time was approximately 2,600 h for the reference surface, whereas the HHP surface only experienced slippery conditions for 1,300 h.

The difference between the calculated hours with risk for frost (230 h) and the observed occasions with slippery conditions (1300 h) can partly be explained by the fact that the calculated values do not take snowfall into account. Snow covered the test surface during a number of days due to cold weather. Furthermore, the traffic on the road transports snow onto the test surface. This snow is detected by the surface state sensor and counted as snow coverage, whereas a few meters away from the measuring point the test surface is snow-free. This is a problem that needs to be handled in the design of HHP systems in order to achieve precise control.

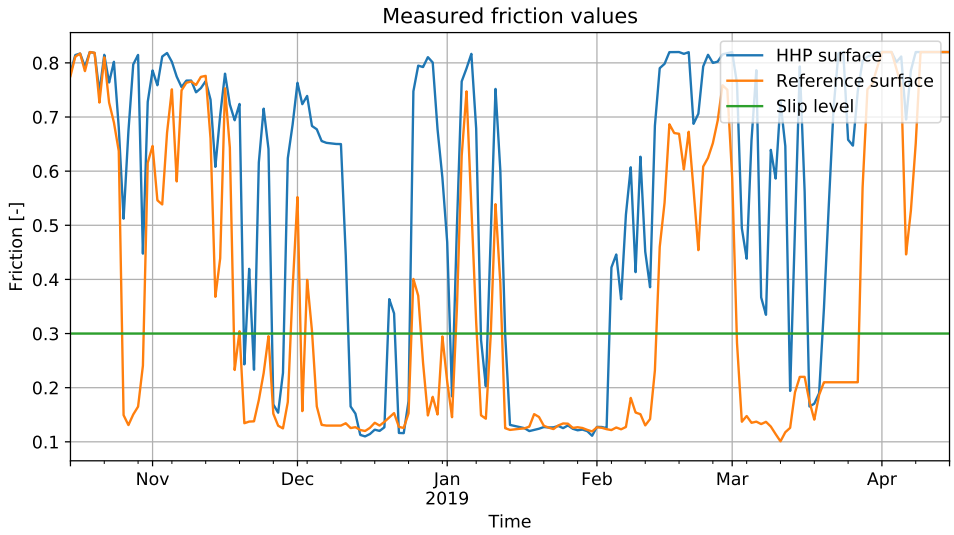

Figure 4.7: Measured friction of test surface and reference surface.

4.2.2 Typical snow fall

During the winter of 2019 there were about 700 hours snow fall spread on 70 days. Most of the snow fall occurred when the air temperature was above -10 $°C$ as can be seen in Figure 4.8. There were approximately 700 h of snowfall, of which 200 h occurred when the temperature was below -10 $°C$. In order to conserve energy the HHP system can therefore be designed to only be active when the air temperature is above -10 $°C$.

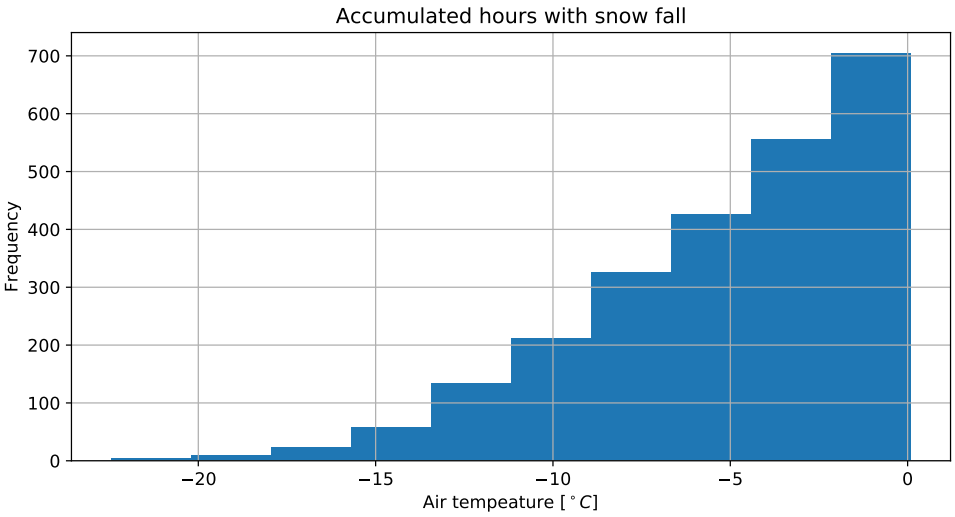

Figure 4.8: Accumulated hours with snow fall at different air temperatures.

One typical snow fall took place during the 9^th of February. In Figure 4.9 a-d the field station can bee seen during the snow fall with observed friction, heat flux,

dew-point temperature, reference surface temperature, HHP surface temperature, and air temperature. The snow started to fall at 3 AM and fell until 5 PM and during the snow fall the air temperature varied between -6 $°C$ and -2 $°C$, see Figure 4.10 a-b.

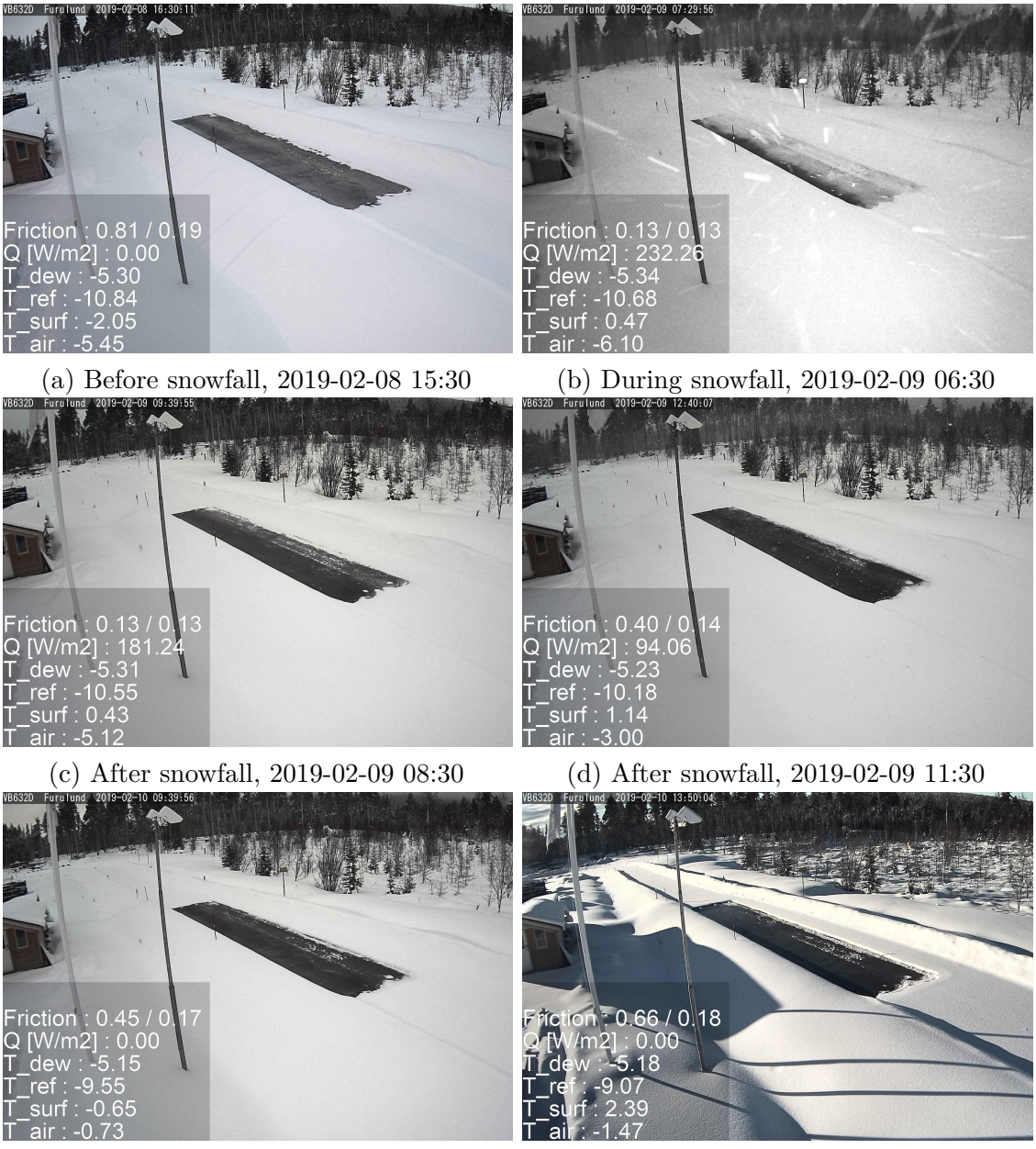

(a) Before snowfall, 2019-02-08 15:30

(b) During snowfall, 2019-02-09 06:30

(c) After snowfall, 2019-02-09 08:30

(d) After snowfall, 2019-02-09 11:30

(e) Day after snowfall, 2019-02-10 9:00

(f) Day after snowfall, 2019-02-10 12:30

Figure 4.9: Photos from a typical snowfall. *Friction*- HHP/reference surface, Q- Heat flux, T_{dew}- dewpoint temperature, T_{ref}- reference surface temperature, T_{surf}- HHP surface temperature, T_{air}- air temperature.

Before the snowfal,l the HHP surface were dry with a friction value of 0.81 compared with the reference surface which were covered by a snow layer, see 4.9a. After a few hours of snowfall the pavements surface were partially covered by snow.

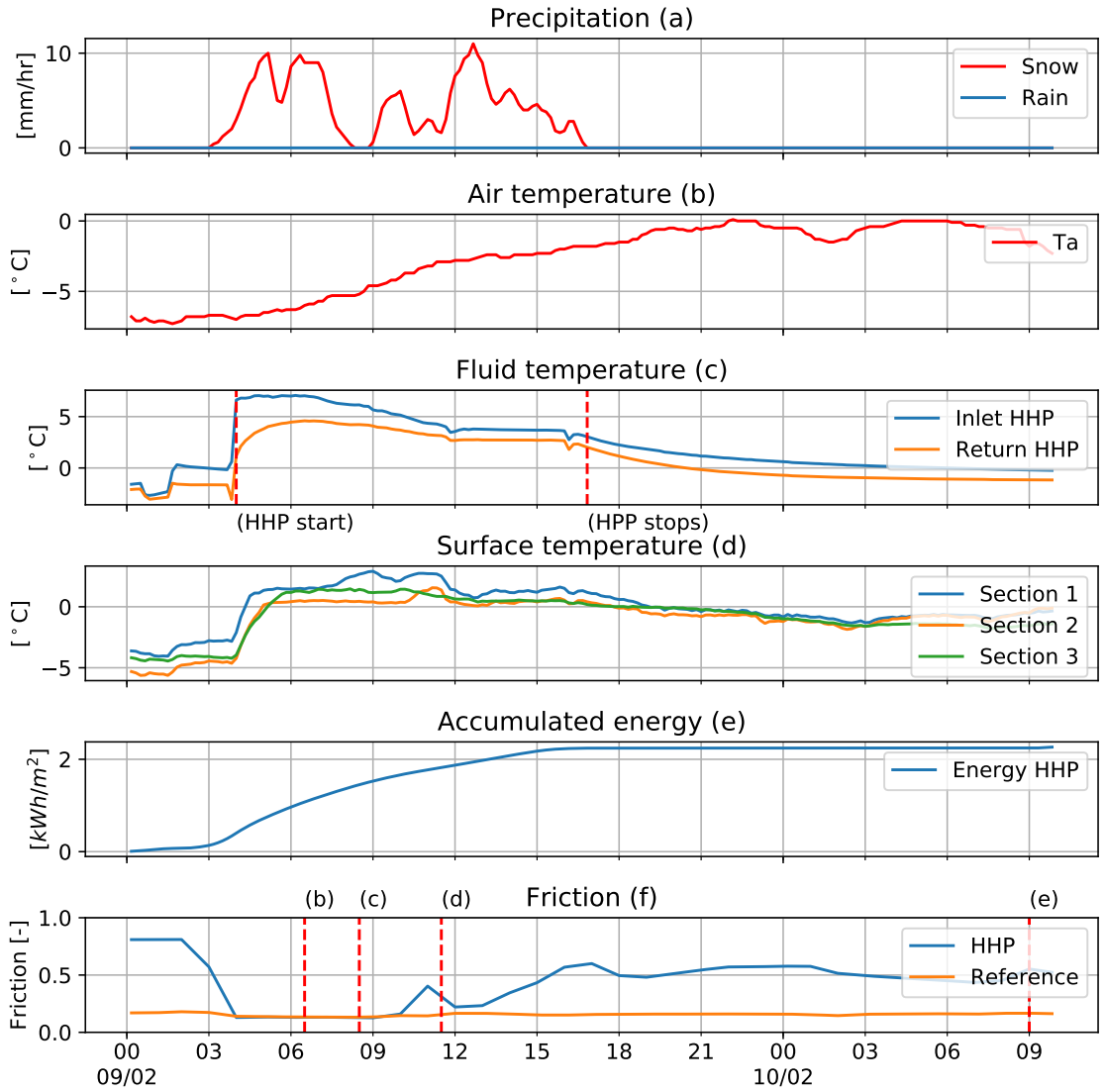

Figure 4.10: Measurements during a snow fall. HHP is started at 2019-02-09 04:00 and stops at 2019-02-09 17:00.

The snow depth increased downs stream of the pipe due to lower fluid temperatures. The friction observed were 0.13 for both the HHP and the refernce surface, see Figure 4.9b. At 8:30 AM there were a thin ice cover on the pavement and by 11:30 AM the ice had started to melt away, see Figure 4.9 c-d. The surface conditions stayed the same into the day after when the surface started to dry up and with a friction above 0.3, see Figure 4.9 e-f.

The HHP system started about an hours after the snowfall since then snow was detected by the surface state sensor. The HHP system was active during the snowfall with a higher supply temperature in the beginning due to the lower air temperature, see Figure 4.10 b-c. The active HHP system rapidly increased the surface temperature of the pavement above 0 $°C$. However, there were about a one hour delay until section 2 and 3 reached above 0 $°C$, see Figure 4.10d.

The active HHP system consumed about 2.3 kWh/m^2 during the snowfall, see Figure 4.10e. With 70 days with snowfall the total energy usage in a year would have been approximately 160 kWh/m^2 if the system would have been active during all of those events.

The HHP system affected the friction of the pavement surface as can be seen in Figure 4.10f. When the snowfall started the friction dropped from 0.81 to 0.13 and after about 6 hours the friction began to increase. It is anticipated that this increase would have been quicker with traffic on the pavement surface since that would have crushed and remove ice, snow, and water from the pavement surface due to splash and spray. After the snowfall the friction was maintained above 0.5, considered an acceptable.

Further adaptation of the control system is necessary to maintain the friction during snowfall and one method would be to implement weather forecasting into the control system. Then the system could pre-heat the pavement before the snowfall and thereby maintaining the friction above 0.3 during a typical snowfall.

Chapter 5

Summary and conclusions

This thesis aims at investigating the function of HHPs in a Scandinavian climate. The thesis is based on both numerical and experimental analyses of an HHP system connected to a BTES. The results indicated that it was possible to harvest more solar energy in the summer than needed during the winter. However, supplementary heating was needed for the cold climate of Östersund.

The experimental part deals with the design and measurements at a field station for an HHP system constructed as a part of these doctoral studies. The data obtained from the field station have been used for verifying a numerical model for HHP systems, called HyRoSim. HyRoSim was used to investigate the efficiency of PSCs and different control strategies of an HHP system.

Paper 2 investigated the influence of two different control strategies on the HHP system in the field station in Östersund. The basic control strategy, based on air temperature, revealed a high energy demand. The energy demand was between 330 and 540 kWh/m^2 with snow and ice cover lasting for 1,300 to 230 h, depending on the snow removal strategy. However, the energy demand can be reduced by using alternative control strategies. The proposed dew point temperature regulation reduced the energy consumption by 62%, while only increasing the period with ice and snow on the pavement by 170 h. Even with the more energy-efficient design, the energy usage is in the range of 125 to 180 kWh/m^2.

The energy demand measured at the field station during the winter of 2018/2019 was 133 kWh/m^2, which is in line with the simulated energy demand of 125 to 180 kWh/m^2. However, only 62 kWh/m^2 of the energy supplied to the HHP system originated from the BTES, because the return temperature from the borehole was lower than the required supply temperature to the HHP of 7 $°C$. A higher supply temperature was needed in order to remove snow and ice from the pavement during cold spells.

The friction and surface conditions on the pavement surface can be improved by an HHP system. The number of hours with risk for frost formation can be reduced from 1340 hours to 230 hours. However, the frost risk do not represent the real surface conditions in a useful way since snowfall and snow transport due to drift or traffic is not included. This is evident when studying the measured friction on the

pavement surface. The measurements indicated that the HHP surface were slippery for 1300 hours while the reference surface were slippery for 2600 hours.

In Paper 4, the function of the HHP as a PSC was studied during the summer of 2018. A total of 245 kWh/m^2 of solar energy was harvested, with a daily mean harvesting load of 70 to 140 W/m^2. The harvested energy had a significant impact on the pavement surface temperature. The mean surface temperature was reduced by 6.4 $^{\circ}C$ in comparison with the reference surface. The lower temperatures can extend the service life of pavement surfaces. However, a lower surface temperature than the ambient air can cause condensation of moisture on the surface. Condensation due to the usage of PSCs has, to our knowledge, not been reported previously. Nevertheless, the risk associated with condensation is considered to be low, because there is no risk of freezing.

The solar efficiency of the PSC during the summer of 2018 was calculated to be 42%, which was higher than in other studies. The higher efficiency of the field station in Sweden can be explained by a shorter pipe distance of 5 cm, high fluid flow rate, and low supply temperature, all of which are factors that increase the solar efficiency. However, the mean air temperature was approximately 2 $^{\circ}C$ higher than average during the summer of 2018. Therefore, a slightly lower solar efficiency should be anticipated for other locations.

In Paper 3, the natural convection within groundwater-filled boreholes was studied. By using recently developed correlations for natural convection, the software PyGfunction was modified to take natural convection into account. This modified software can be used to design shallow geothermal systems without the need to rely on estimations of the thermal conductivity of the filling material to calculate the borehole resistance.

Locations that could be suitable for installing an HHP system can be identified by performing interviews with the local winter maintenance organisations. They commonly have detailed knowledge about the problem spots in their areas of operation. The identified locations can thereafter be investigated through a preliminary design phase.

Based on the experimental and numerical results presented herein, it can be concluded that it is feasible to design HHP systems to use low-temperature ($<$10 $^{\circ}C$) sources and at the same time achieve a substantial improvement in the surface conditions.

Chapter 6

Further research

- Performance of hydronic pavements

  Further monitoring of the field station is required to evaluate the performance of the HPP system and to determine for how many hours the HP system is allowed to fail, as this is crucial for the design of the system. The system requires substantially more power and energy during extreme weather. However, the amount of energy is limited, which means the performance of the system will be reduced. A study should be performed to determine acceptable risk levels. A qualitative interview study should also be performed.

- Control system

  The results reveal that the dew point temperature should be used as a part of the control system for hydronic pavements, and weather forecasting can be used to reduce the energy demand of the HHP system. However, the addition of a weather forecasting model and an algorithm to select the appropriate supply temperature should be implemented into the control system of the field station.

- Cost–benefit analyses

  The cost of implementing an HHP system needs to be evaluated. A cost–benefit analysis must be performed in order to determine when an HHP should be used. A methodology should be developed such that financial evaluations of the viability of the proposed concept can be performed.

- Supplementary heat sources

  Supplementary heat sources are needed in locations with insufficient energy harvesting. Heat pumps should be implemented into the HyRoSim software .

- Durability and maintenance

  One question that needs to be answered pertains to the lifetime of the pipes embedded in the pavement. Therefore, there is a need for research on their mechanical durability and on how maintenance of the pipes embedded in the pavement should be performed.

Bibliography

Adl-Zarrabi, Bijan, Babak Ebrahimi, Mohammed Hoseini, Josef Johnsson, Raheb Mirzanamadi, and Maria Taljegard (2016). "Safe and Sustainable Coastal Highway Route E39". In: *Transportation Research Procedia* 14, pp. 3350–3359. ISSN: 23521465. DOI: 10.1016/j.trpro.2016.05.286 (cit. on p. 5).

Adlam, Thomas Napier (1950). *Snow melting; design, installation and control of systems for melting snow*. New York. URL: http://catalog.hathitrust.org/Record/001611433%20http://hdl.handle.net/2027/mdp.39015004531748%20http://hdl.handle.net/2027/wu.89088906359 (cit. on pp. 4, 7).

Almkvist, Esben and Josef Johnsson (2017). *Identifying critical road sections related to winter road maintenance*. Tech. rep. Göteborg, p. 22. URL: http://publications.lib.chalmers.se/publication/248093-identifying-critical-road-sections-related-to-winter-road-maintenance (cit. on p. 8).

Andersson, Anna K. (2010). "Winter Road Conditions and Traffic Accidents in Sweden and UK: Present and Future Climate Scenarios". Doktorsavhandling. Göteborg: Göteborg University. URL: https://gupea.ub.gu.se/handle/2077/21547 (cit. on p. 3).

Andersson, Olof and Signhild Gehlin (2018). *State-of-the-Art: Sweden Quality Management in Design, Construction and Operation of Borehole Systems*. Tech. rep. Stockholm: Svenskt Geoenergicentrum, pp. 1–37. URL: http://media.geoenergicentrum.se/2018/06/Andersson%7B%5C_%7DGehlin%7B%5C_%7D2018%7B%5C_%7DState-of-the-Art-report-Sweden-for-IEA-ECES-Annex-27.pdf (cit. on p. 22).

Arvidsson, Anna, Árni Jacobsen, Bård Nonstad, Freddy Knudsen, Kenneth Natanaelsson, Olav Korsaksel, Otto Kärki, Skúli Thordarson, and Tine Damkjaer (2018). *Vintervåghållning i de nordiska länderna: Statusrapport 2018*. Tech. rep. 1. NVF, pp. 1–60 (cit. on p. 4).

Carlsson, Anna, Beshara Sawaya, Jordanka Kovaceva, and Marianne Andersson (2018). *Skadereducerande Effekt av Uppvärmda Trottoarer , Gång- och Cykelstråk*. Tech. rep. Borlänge: Trafikverket (cit. on pp. 7, 8).

Chalmers University of Technology (2013). *Chalmers helps Norway bridge the fjords*. URL: https://www.chalmers.se/en/departments/cee/news/Pages/Chalmers-helps-Norway-bridge-the-fjords.aspx (visited on 12/19/2016) (cit. on p. 5).

Chen, Jiaqi, Hao Wang, and Pengyu Xie (July 2019). "Pavement temperature prediction: Theoretical models and critical affecting factors". In: *Applied Thermal Engi-*

neering 158.May, p. 113755. ISSN: 13594311. DOI: 10.1016/j.applthermaleng.2019.113755 (cit. on pp. 15, 25).

Cimmino, Massimo (Oct. 2017). "A finite line source simulation model for geothermal systems with series- and parallel-connected boreholes and independent fluid loops". In: *Journal of Building Performance Simulation*, pp. 1–19. ISSN: 1940-1493. DOI: 10.1080/19401493.2017.1381993 (cit. on pp. 12, 22).

Cimmino, Massimo (2018). *pygfunction: A g-function calculator for Python*. DOI: 10.5281/zenodo.1195039. URL: https://github.com/MassimoCimmino/pygfunction (cit. on p. 11).

Cimmino, Massimo and Michel Bernier (2014). "A semi-analytical method to generate g-functions for geothermal bore fields". In: *International Journal of Heat and Mass Transfer* 70, pp. 641–650. ISSN: 00179310. DOI: 10.1016/j.ijheatmasstransfer.2013.11.037 (cit. on pp. 12, 22).

Claesson, J and G Hellström (2011). "Multipole method to calculate borehole thermal resistances in a borehole heat exchanger". English. In: *HVAC and R Research* 17.6, pp. 895–911. DOI: 10.1080/10789669.2011.609927 (cit. on p. 22).

Claesson, Johan and Alain Dunand (1983). *Heat extraction from the ground by horizontal pipes: a mathematical analysis*. Tech. rep. Lund (cit. on p. 20).

Denby, B R et al. (2013). "A coupled road dust and surface moisture model to predict non-exhaust road traffic induced particle emissions (NORTRIP). Part 2: Surface moisture and salt impact modelling". In: *Atmospheric Environment* 81.0, pp. 485–503. DOI: http://dx.doi.org/10.1016/j.atmosenv.2013.09.003 (cit. on pp. 17–19).

Ebrahim Abu El-Maaty, Ahmed (2018). "Temperature Change Implications for Flexible Pavement Performance and Life". In: *International Journal of Transportation Engineering and Technology* 3.1, p. 1. ISSN: 2575-1743. DOI: 10.11648/j.ijtet.20170301.11 (cit. on p. 40).

Eugster, Walter J (2002). "SERSO PLUS – Neue Wege in der Belagsbeheizung". In: *Geothermische Energie : Mitteilungsblatt der Geothermischen Vereinigung e.V.* 10.38-39 (cit. on p. 4).

Eugster, Walter J (2007). "Road and Bridge Heating Using Geothermal Energy Overview and Examples." In: *European Geothermal Congress* June, p. 5 (cit. on p. 4).

Fay, Laura and Xianming Shi (2012). "Environmental Impacts of Chemicals for Snow and Ice Control: State of the Knowledge". In: *Water, Air, & Soil Pollution* 223.5, pp. 2751–2770. ISSN: 0049-6979. DOI: 10.1007/s11270-011-1064-6 (cit. on p. 4).

Gehlin, Signhild (2002). "Thermal response test method development and evaluation". PhD thesis. Luleå University of Technology. ISBN: 1402-1544. DOI: LTU-DT-0239-SE (cit. on pp. 36, 37).

Gehlin, Signhild and Goran Hellstrom (2003). "Comparison of four models for thermal response test evaluation". English. In: *ASHRAE Transactions* 109, p. 131. ISSN: 00012505 (cit. on p. 37).

Guldentops, Gert, Alireza Mahdavi Nejad, Cedric Vuye, Wim Van den bergh, and Nima Rahbar (2016). "Performance of a pavement solar energy collector: Model

development and validation". In: *Applied Energy* 163, pp. 180–189. ISSN: 03062619. DOI: 10.1016/j.apenergy.2015.11.010 (cit. on p. 26).

Hagentoft, Carl-Eric (2001). *Introduction to Building Physics*. en. Lund: Studentlitteratur. ISBN: 9144018967 (cit. on pp. 15, 17, 18).

Jansson, C, E Almkvist, and P E Jansson (2006). "Heat balance of an asphalt surface: observations and physically-based simulations". In: *Meteorological Applications* 13.2, pp. 203–212. DOI: 10.1017/S1350482706002179 (cit. on p. 25).

Javed, Saqib, Jeffrey D Spitler, and Per Fahlén (2011). "An experimental investigation of the accuracy of thermal response tests used to measure ground thermal properties". In: *ASHRAE Transactions* 117.1, pp. 13–21. ISSN: 0001-2505 (cit. on p. 38).

Johansson, Alf (2000). *Vinterdrift vägar, gator, järnvägar och flygfält*. Ed. by Alf Johansson. Rapport nr 2. Göteborg: Chalmers Lindholmen University (cit. on p. 3).

Johnsson, Josef (2017a). *Winter road maintenance a review*. Tech. rep. Göteborg: Chalmers University of Technology (cit. on pp. 3, 7).

Johnsson, Josef (2017b). "Winter Road Maintenance using Renewable Thermal Energy". PhD thesis. Gothenburg: Chalmers University of Technology. URL: http://publications.lib.chalmers.se/publication/248119-winter-road-maintenance-using-renewable-thermal-energy (cit. on pp. 11, 22, 27).

Johnsson, Josef and Bijan Adl-Zarrabi (Nov. 2019). "Modelling and evaluation of groundwater filled boreholes subjected to natural convection". In: *Applied Energy* 253, p. 113555. ISSN: 03062619. DOI: 10.1016/j.apenergy.2019.113555 (cit. on p. 31).

Karlsson, Henrik (Apr. 2010). "Embedded Water-based Surface Heating Part 1: Hybrid 3D Numerical Model". In: *Journal of Building Physics* 33.4, pp. 357–391. ISSN: 1744-2591. DOI: 10.1177/1744259109360151 (cit. on pp. 15, 19, 21).

Ketzel, Matthias, Gunnar Omstedt, Christer Johansson, Ingo Düring, Lars Gidhagen, Achim Lohmeyer, Ruwim Berkowicz, and Peter Wåhlin (2007). "Estimation and validation of PM 2.5 /PM 10 exhaust and non-exhaust emission factors for street pollution modelling". In: *Atmospheric Environment* 41.40, pp. 9370–9385 (cit. on p. 4).

Klein-Paste, Alex (June 2008). "Physical Processes That Affect Runway Surface Conditions During Winter Time: A Conceptual Model". In: *Transportation Research E-Circular*. Ed. by Ann E. Petty. E-C126. Washington, D.C.: Transportation Research Board, pp 537–543 (cit. on p. 3).

Knollhoff, D. S., E. S. Takle, W. A. Gallus, D. Burkheimer, and D. McCauley (Dec. 2003). "Evaluation of a frost accumulation model". In: *Meteorological Applications* 10.4, pp. 337–343. ISSN: 1350-4827. DOI: 10.1017/S1350482703001026 (cit. on p. 27).

Knudsen, Freddy, Kenneth Natanaelsson, Anna Arvidsson, Otto Kärki, Árni Jacobsen, Gudmundur Gudmundsson, Bård Nonstad, and Reitan Knut Magne (2016). *Vintertjeneste i de Nordiske land: Statusrapport 2016*. Tech. rep. Drift og vedlikehold, prosjekt vinterteknologi. URL: http://www.nvfnorden.org/library/

Files/Land/Styrelse-NVF/Rapporter/2016/Stausrapport%202016.pdf (cit. on p. 4).

Konzelmann, Thomas, Roderik S W van de Wal, Wouter Greuell, Richard Bintanja, Edwin A C Henneken, and Ayako Abe-Ouchi (1994). "Parameterization of global and longwave incoming radiation for the Greenland Ice Sheet". In: *Global and Planetary Change* 9.1, pp. 143–164. ISSN: 0921-8181. DOI: https://doi.org/10.1016/0921-8181(94)90013-2 (cit. on p. 17).

Kuemmel, David and Rashad Hanbali (1992). *Accident analysis of ice control operations: Final Report*. Tech. rep. Milwaukee: Department of Civil and Environmental Engineering (cit. on pp. 3, 4).

Li, H., J. Harvey, and A. Kendall (2013). "Field measurement of albedo for different land cover materials and effects on thermal performance". In: *Building and Environment* 59, pp. 536–546. ISSN: 03601323. DOI: 10.1016/j.buildenv.2012.10.014 (cit. on p. 25).

Lindqvist, S, J-O Mattson, and Et al. (1983). *Vägklimatologi*. Tech. rep. Borlänge: BERGAB Klimatundersökningar (cit. on p. 4).

Loomans, M, H Oversloot, and A de Bondt (2003). "Design tool for the thermal energy potential of asphalt pavements". In: *Eighth International IBPSA Conference*. Eindhoven, Netherlands, pp. 745–752 (cit. on pp. 26, 39).

Lund, John W (2000). "Pavement Snow Melting". In: *Geo-Heat Center Quarterly Bulletin* 21.No. 2 (cit. on p. 4).

Lund, John W. and Tonya L. Boyd (2016). "Direct utilization of geothermal energy 2015 worldwide review". In: *Geothermics* 60, pp. 66–93. ISSN: 03756505. DOI: 10.1016/j.geothermics.2015.11.004 (cit. on p. 7).

Lysbakken, Kai Rune (2013). "Salting of Winter Roads : The Quantity of Salt on Road Surfaces after Application". eng. PhD thesis. Norwegian University of Science and Technology. ISBN: 978-82-471-4551-7. URL: http://www.diva-portal.org/smash/get/diva2:660746/FULLTEXT02.pdf (cit. on pp. 3, 4).

Magnusson, Rolf (1977). "Uppvärmning av vägar : energiförbrukning och effektbehov som funktion av klimatfaktorer, konstruktion, krav på ytförhålland och uppvärmningsstrategi". PhD thesis. Göteborg: Chalmers tekniska högskola, p. 143. ISBN: 99-0139857-6 (cit. on p. 4).

Melinder, Åke (2007). "Thermophysical Properties of Aqueous Solutions Used as Secondary Working Fluids". eng. Doctoral Thesis. Royal Institute of Technology, KTH. URL: http://www.diva-portal.org/smash/record.jsf?pid=diva2%7B%5C%%7D3A12169%7B%5C&%7Ddswid=-3987 (cit. on p. 35).

Minsk, L David (1998). *Snow and ice control manual for transportation facilities*. New York: McGraw-Hill. ISBN: 0070428093; 9780070428096 (cit. on p. 3).

Mirzanamadi, Raheb (2019). "Utilizing solar energy for anti-icing road surfaces using hydronic heating pavement with low temperature". Doktorsavhandlingar Ny serie: 4535. Chalmers University of Technology. ISBN: 9789175978543 (cit. on p. 44).

Mirzanamadi, Raheb, Pär Johansson, and Sotirios A. Grammatikos (2018). "Thermal properties of asphalt concrete: A numerical and experimental study". In: *Construction and Building Materials* 158, pp. 774–785. ISSN: 09500618. DOI: 10.1016/j.conbuildmat.2017.10.068 (cit. on p. 35).

Narsilio, Guillermo Andres and Lu Aye (2018). "Low Carbon Energy Supply". In: *Low Carbon Energy Supply*. Ed. by Atul Sharma, Amritanshu Shukla, and Lu Aye. Green Energy and Technology. Singapore: Springer Singapore. ISBN: 978-981-10-7325-0. DOI: 10.1007/978-981-10-7326-7 (cit. on p. 22).

Nasir, Diana S.N.M., Ben Richard Hughes, and John Kaiser Calautit (2016). "A CFD analysis of several design parameters of a road pavement solar collector (RPSC) for urban application". In: *Applied Energy*. ISSN: 03062619. DOI: 10.1016/j.apenergy.2016.04.002 (cit. on p. 25).

Nordin, Lina (2015). "Energy Efficiency In Winter Road Maintenance A Road Climatological Perspective". PhD thesis. Gothenburg. ISBN: 978-91-628-9447-4 (cit. on pp. 4, 7).

Norrman, J, M Eriksson, and S Lindqvist (2000). "Relationships between road slipperiness, traffic accident risk and winter road maintenance activity". In: *Climate Research* 15.3, pp. 185–193. ISSN: 0936-577X. DOI: 10.3354/cr015185 (cit. on p. 3).

Nuijten, Anne D W (May 2016). "Runway temperature prediction, a case study for Oslo Airport, Norway". In: *Cold Regions Science and Technology* 125, pp. 72–84. ISSN: 0165232X. DOI: 10.1016/j.coldregions.2016.02.004 (cit. on p. 35).

Orring, Anna (2012). *Sommarvärme mot blixthalkan | NYTEKNIK*. URL: http://www.nyteknik.se/fordon/sommarvarme-mot-blixthalkan-6405769 (visited on 12/20/2016) (cit. on p. 5).

Pahud, Daniel (2007). *Serso, stockage saisonnier solaire pour le dégivrage d'un pont*. Tech. rep. Bern (cit. on p. 4).

Pan, Pan, Shaopeng Wu, Yue Xiao, and Gang Liu (Aug. 2015). "A review on hydronic asphalt pavement for energy harvesting and snow melting". English. In: *Renewable and Sustainable Energy Reviews* 48, pp. 624–634. ISSN: 13640321. DOI: 10.1016/j.rser.2015.04.029 (cit. on p. 4).

Sass, Bent H. (Dec. 1992). "A Numerical Model for Prediction of Road Temperature and Ice". In: *Journal of Applied Meteorology* 31.12, pp. 1499–1506. ISSN: 0894-8763. DOI: 10.1175/1520-0450(1992)031<1499:ANMFPO>2.0.CO;2 (cit. on p. 17).

Spitler, Jeffrey D, Saqib Javed, and Randi Kalskin Ramstad (2016). "Natural convection in groundwater-filled boreholes used as ground heat exchangers". In: *Applied Energy* 164, pp. 352–365. ISSN: 0306-2619. DOI: https://doi.org/10.1016/j.apenergy.2015.11.041 (cit. on pp. 23, 24).

Statens Vegvesen (2013). *Vegvesen-avtale med Chalmers*. URL: http://www.vegvesen.no/om+statens+vegvesen/presse/Pressemeldingsarkiv/Vegdirektoratet/vegvesen-avtale-med-chalmers (visited on 12/19/2016) (cit. on p. 5).

Sundberg, Jan (2012). *Halkfria vägar: Solvärme och värmelagring för miljöanpassad halkbekämpning*. Tech. rep. Borlänge, p. 35 (cit. on p. 5).

Sundberg, Jan (2019). *Halkfria vägar - Etapp 3 Byggande testyta med geoenergi Mål, motiv och dokumentation*. Tech. rep. Trafikverket (cit. on p. 33).

Sundberg, Jan and Peter Lidén (2014). *Halkfria vägar – Etapp 2. Energi- och systemanalys med kostnader. Solvärme och värmelagring för miljöanpassad halkbekämpning*. Tech. rep. Borlänge. URL: https://online4.ineko.se/trafikverket/Product/Detail/45758 (cit. on pp. 5, 9).

U.S Environmental Protection Agency (2012). "Cool Pavements". In: *Reducing Urban Heat Islands: Compendium of Strategies*, pp. 1–23. ISBN: 978-1-4244-7159-1. DOI: 10.1175/1520-0450(2002)041<0792:THFIUA>2.0.CO;2 (cit. on p. 25).

Usman, Taimur, Liping Fu, and Luis F Miranda-Moreno (Nov. 2010). "Quantifying safety benefit of winter road maintenance: accident frequency modeling." In: *Accident; analysis and prevention* 42.6, pp. 1878–87. ISSN: 1879-2057. DOI: 10.1016/j.aap.2010.05.008 (cit. on p. 3).

Valavanidis, Athanasios, Konstantinos Fiotakis, and Thomais Vlachogianni (Dec. 2008). "Airborne Particulate Matter and Human Health: Toxicological Assessment and Importance of Size and Composition of Particles for Oxidative Damage and Carcinogenic Mechanisms". In: *Journal of Environmental Science and Health, Part C* 26.4, pp. 339–362. ISSN: 1059-0501. DOI: 10.1080/10590500802494538 (cit. on p. 4).

Wallman, Carl-Gustaf, Gudrun Öberg, and Peter Wretling (1997). *Effects of winter road maintenance: state-of-the-art*. Tech. rep. Linköping (cit. on p. 3).

WHO (2015). *Global Status Report on Road Safety 2015*. Tech. rep., p. 340 (cit. on p. 3).

Ye, Zhirui, Jianlin Wu, Nabil El Ferradi, and Xianming Shi (Jan. 2013). "Anti-icing for key highway locations: fixed automated spray technology". In: *Canadian Journal of Civil Engineering* 40.1, pp. 11–18. ISSN: 0315-1468. DOI: 10.1139/cjce-2012-0226 (cit. on p. 4).

Part II

Appended papers